The Astronomical Journal, 129:251–266, 2005 January

CHEMICAL ABUNDANCES FOR SEVEN GIANT STARS IN M68 (NGC 4590): A GLOBULAR CLUSTER WITH ABNORMAL SILICON AND TITANIUM ABUNDANCES

Jae-Woo Lee,[1] Bruce W. Carney,[2,3] and Michael J. Habgood[2]
Received 2004 September 7; accepted 2004 September 22

ABSTRACT

We present a detailed chemical abundance study of seven giant stars in M68, including six red giants and one post–asymptotic giant branch (AGB) star. We find significant differences in the gravities determined using photometry and those obtained from ionization balance, which suggests that non-LTE (NLTE) affects are important for these low-gravity, metal-poor stars. We adopt an iron abundance using photometric gravities and Fe II lines to minimize those effects, finding $[\mathrm{Fe/H}] = -2.16 \pm 0.02$ ($\sigma = 0.04$). For element-to-iron ratios, we rely on neutral lines versus Fe I and ionized lines versus Fe II (except for [O/Fe]) to also minimize NLTE effects. We find variations in the abundances of sodium among the program stars. However, there is no correlation (or anticorrelation) with the oxygen abundances. Furthermore, the post-AGB star has a normal (low) abundance of sodium. Both of these facts add further support to the idea that the variations seen among some light elements within individual globular clusters arise from primordial variations and not from deep mixing. M68, like M15, shows elevated abundances of silicon compared with other globular clusters and comparable-metallicity field stars. But M68 deviates even more in showing a relative underabundance of titanium. We speculate that in M68 titanium is behaving like an iron-peak element rather than its more commonly observed adherence to enhancements seen in the so-called α-elements such as magnesium, silicon, and calcium. We interpret this result as implying that the chemical enrichment seen in M68 may have arisen from contributions from supernovae with somewhat more massive progenitors than those that contribute to abundances normally seen in other globular clusters. The neutron capture elements barium and europium vary among the stars in M15, according to earlier work by Sneden et al., but [Ba/Eu] is relatively constant, suggesting that both elements arise in the same nucleosynthesis events. M68 shares the same [Ba/Eu] ratio as the stars in M15, but the average abundance ratio of these elements, as well as lanthanum, are lower in M68 relative to iron than in M15, implying a slightly weaker contribution of *r*-process nucleosynthesis in M68.

Key words: Galaxy: halo — globular clusters: individual (M68, NGC 4590) — stars: abundances

1. INTRODUCTION

Globular clusters in our Galaxy do not define a single homogeneous population with a single history. In his pioneering work, Zinn (1985) subdivided the globular clusters into the "halo" and the "thick-disk" groups at $[\mathrm{Fe/H}] = -0.8$. The halo clusters have an essentially spherical distribution about the Galactic center, and they constitute a pressure-supported system (a small rotational velocity and a larger velocity dispersion), while the thick-disk clusters have a highly flattened spatial distribution and constitute a rotationally supported system (a larger rotational velocity and a smaller velocity dispersion). Searle & Zinn (1978) and Lee et al. (1994) suggested that the inner halo globular clusters exhibit a tight horizontal branch (HB) morphology versus [Fe/H] relation, while the outer halo globular clusters show the second-parameter phenomenon (i.e., a larger scatter in HB type[4] at a given [Fe/H]). Subsequently, Zinn (1993) subdivided the halo clusters into two groups. The "old halo" group obeys the same HB type versus [Fe/H] relationship as the inner halo clusters, while the "younger halo" group deviates from this relationship by a significant amount (see Fig. 1). Zinn (1993) and Da Costa & Armandroff (1995) argued that the old and the younger halo groups have different kinematic properties and that the old halo group has a prograde mean rotation velocity with a smaller velocity dispersion, while the younger halo group has a retrograde mean rotation velocity about the Galactic center with a larger velocity dispersion. They suggested that the old halo group formed during the collapse that led ultimately to the formation of the Galactic disk and the younger halo group were accreted later. If so, one would expect to see signatures of different chemical enrichment histories carved in spectra of stars in globular clusters. For example, one might be able to investigate the early form of the initial mass function (IMF) by studying abundances of stellar mass–sensitive elements (see discussion and references in McWilliam 1997).

An alternative perspective on younger halo and old halo clusters is that of dissolved and accreted dwarf galaxies. For example, Freeman (1993) suggested that the massive and chemically unusual globular cluster ω Cen might be the remnant nucleus of an accreted dwarf galaxy. Lynden-Bell & Lynden-Bell (1995) noted the possible alignments of orbital poles of some globular clusters such that they might comprise a "spoor" (more commonly referred to as a "stream") of clusters. While the specific details have not found support, the idea has been

[1] Department of Astronomy and Space Science, Astrophysical Research Center for the Structure and Evolution of the Cosmos, Sejong University, 98 Gunja-Dong, Gwangjin-Gu, Seoul 143-747, Korea; jaewoo@arcsec.sejong.ac.kr.

[2] Department of Physics and Astronomy, University of North Carolina, Chapel Hill, NC 27599-3255; bruce@physics.unc.edu, mjames@astro.unc.edu.

[3] Visiting Astronomer, Cerro Tololo Inter-American Observatory, National Optical Astronomy Observatory (NOAO), which is operated by the Association of Universities for Research in Astronomy (AURA), Inc., under cooperative agreement with the National Science Foundation (NSF).

[4] HB type is defined to be $(B - R)/(B + V + R)$, where B, V, and R are the numbers of blue HB stars, RR Lyrae variables, and red HB stars, respectively (Lee et al. 1990).

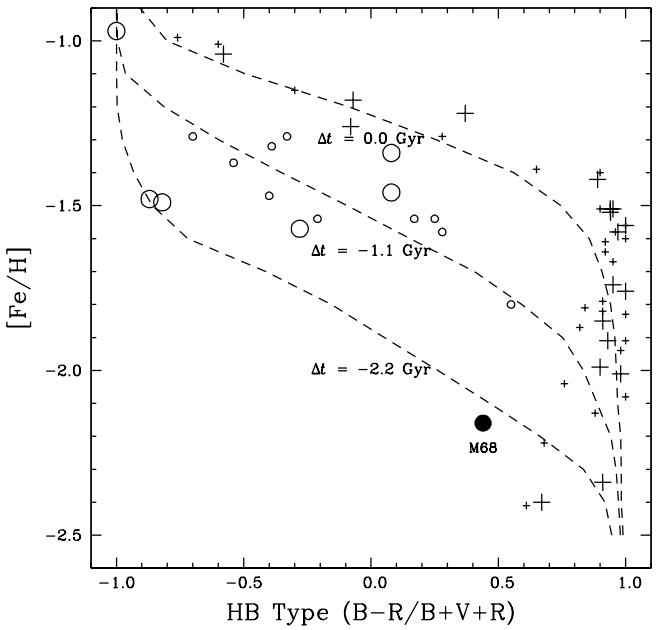

FIG. 1.—HB type vs. [Fe/H] (HB isochrones) of halo globular clusters (Da Costa & Armandroff 1995) and M68. Plus signs represent old halo clusters, and open circles younger halo clusters, where large plus signs and open circles denote clusters studied using high-resolution spectroscopy (see also Fig. 2). HB isochrones for $\Delta t = 0.0$, -1.1, and -2.2 Gyr (with respect to the mean age of old halo globular clusters) are also shown with dashed lines (Rey et al. 2001).

demonstrated very nicely by Dinescu et al. (2000), who found a clear dynamical relationship between the space motions of the young globular cluster Pal 12 and the Sagittarius dwarf galaxy. Indeed, other globular clusters may also be associated with this particular accretion event (NGC 5634: Bellazzini et al. 2002; NGC 4147: Bellazzini et al. 2003; Pal 2: Majewski et al. 2004). Yoon & Lee (2002) have similarly speculated on a dynamical relationship between some metal-poor globular clusters, including M68. Yoon & Lee (2002) suggested that M68 was a member of a satellite galaxy and accreted later to our Galaxy, resulting in a planar motion of several metal-poor clusters, including M15 and M92.

Dynamical evolution in the Galaxy can eventually dissolve streams, making their detection difficult. However, an interesting alternative exists, called "chemical tagging." As Freeman & Bland-Hawthorn (2002) discussed, stars born in galaxies whose star formation histories differ from those that have created the bulk of the Galaxy's stars may still be discernible in unusual element-to-iron ratios. Indeed, Cohen (2004) has found a compelling link between Pal 12 and the Sagittarius dwarf. Detailed chemical abundances of globular clusters may yet become the principal means of identifying historical links between stars and clusters that are now widely dispersed in our Galaxy.

M68 (NGC 4590) is part of the younger halo, according to its HB type with respect to its metallicity, and is located 10 kpc from the Galactic center. Dinescu et al. (1999) found that the cluster's Galactic orbit carries it rather far from the Galactic center, perhaps as far as 30 kpc. As shown in Figure 1, globular clusters with $[\mathrm{Fe/H}] \leq -2.0$ have HB types that are greater than 0.6, with the exception of M68. If age is the second parameter,[5] M68 represents the low-metallicity tail of the younger halo globular clusters. The absolute age of M68 appears to be slightly younger than the oldest globular clusters in our Galaxy. Rosenberg et al. (1999) argued that M68 is coeval to or slightly younger than those of the oldest halo globular clusters, while VandenBerg (2000) maintained that the age of M68 is less than that of M92, one of the oldest globular clusters in our Galaxy, by ≈15%.

The previous metallicity estimates of M68 as follows. Zinn & West (1984) and Zinn (1985) adopted $[\mathrm{Fe/H}] = -2.09$. Gratton & Ortolani (1989) observed two stars in M68 with one being in common with this study. They derived elemental abundances for 11 species, including iron, finding $[\mathrm{Fe/H}] = -1.92$. However, because of the low resolving power ($R = 15{,}000$) of their spectra, their equivalent width (EW) measurements were vulnerable to line blending. Minniti et al. (1993) observed two stars in M68, one of them in common with Gratton & Ortolani (1989) and this study, finding $[\mathrm{Fe/H}] = -2.17$. Minniti et al. (1996) also discussed oxygen and sodium abundances of the cluster. Finally, Rutledge et al. (1997) observed the infrared Ca II triplet for 19 stars and obtained $[\mathrm{Fe/H}] = -2.11 \pm 0.03$ using the Zinn & West (1984) [Fe/H] scale.

In this paper, we explore the detailed elemental abundances for seven giant stars in M68. One is a probable asymptotic giant branch (AGB) star, and the remaining six are red giant branch (RGB) stars. This study is tied directly to that of Lee & Carney (2002) with the same instrument setups and analysis methods.

2. OBSERVATIONS AND DATA REDUCTION

The observations were carried out on 1996 May 4–7. We selected our program RGB stars from the BV photometry of Walker (1994). The positions of our target giant stars on the color-magnitude diagram (CMD), along with bright stars in M68, are shown in Figure 2. In Table 1, we provide identifications (Alcaino 1977; Harris 1975; Walker 1994), position (Cutri et al. 2000), V magnitudes, $B - V$ colors (Walker 1994), and K magnitudes (Frogel et al. 1983; Cutri et al. 2000) of our target stars. Please note that the 2MASS K magnitudes have

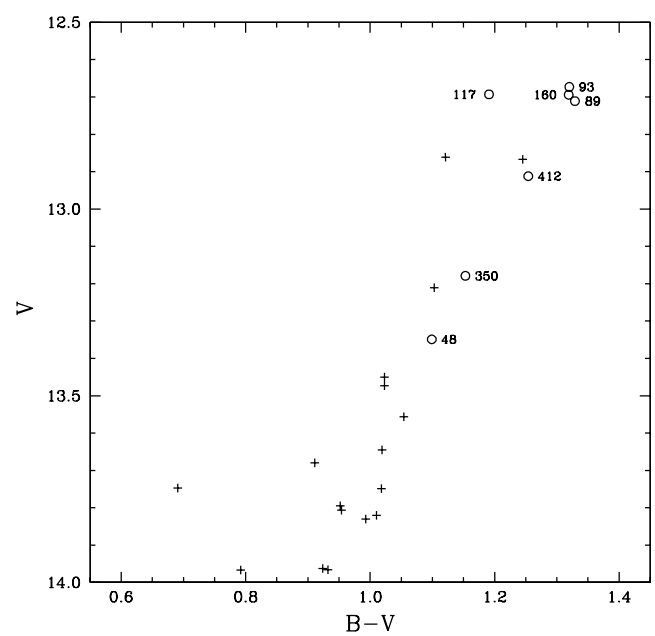

FIG. 2.—CMD of M68 with photometry from Walker (1994), showing the positions of our program stars.

[5] The "second parameter" is the disputed variable that, in addition to mean metallicity, determines the HB type of a cluster.

TABLE 1
JOURNAL OF OBSERVATIONS

Star[a]		Position (J2000)[b]								
W	Alt.	α	δ	V[c]	$(B-V)$[c]	K[d]	K[e]	Date/Time	t_{exp} (minutes)	S/N
93	I-82	12 39 20.9	−26 46 54	12.67	1.32	9.53	9.57	1996 May 4	120	170
117	ZNG 2[f]	12 39 22.5	−26 45 12	12.69	1.19	9.73	9.73	1996 May 6	120	115
160	I-260	12 39 24.7	−26 43 33	12.69	1.32	9.52	9.53	1996 May 4	120	160
89	A-14	12 39 20.8	−26 41 39	12.71	1.33	9.55	9.57	1996 May 4	120	160
412	I-144	12 39 30.8	−26 47 53	12.91	1.25	9.88	9.90	1996 May 6	170	140
350	...	12 39 29.4	−26 44 23	13.18	1.15	...	10.22	1996 May 5	190	140
48	...	12 39 15.9	−26 45 15	13.35	1.10	...	10.53	1996 May 7	130	90

NOTE.—Units of right ascension are hours, minutes, and seconds, and units of declination are degrees, arcminutes, and arcseconds.
[a] "W" from Walker (1994), "A" from Alcaino (1977), and "I" from Harris (1975).
[b] Positional data from 2MASS (Cutri et al. 2000).
[c] Walker (1994).
[d] Frogel et al. (1983).
[e] 2MASS photometric data using the CIT system (Cutri et al. 2000).
[f] An ultraviolet bright star (Zinn et al. 1972).

been converted to the CIT system (Cutri et al. 2000) and are in good agreement with those of Frogel et al. (1983). We obtained high signal-to-noise ratio (S/N $\geq$ 90 pixel^{-1}) echelle spectra using the Cerro Tololo Inter-American Observatory 4 m telescope and its Cassegrain echelle spectrograph. The Tek 2048 $\times$ 2048 CCD, 31.6 line mm^{-1} echelle grating, long red camera, and G181 cross-disperser were employed for our observations. The slit width was 150 μm, or about 1″.0, projected to 2.0 pixels, yielding an effective resolving power $R = 28{,}000$. Each spectrum had complete spectral coverage from 5420 to 7840 Å. All program star observations were accompanied by flat-lamp, Th-Ar lamp, and bias frames.

The raw data frames were trimmed, bias-corrected, and flat-fielded using the IRAF[6] ARED and CCDRED packages. The scattered light was also subtracted using the APSCATTER task in ECHELLE package. The echelle apertures were then extracted to form one-dimensional spectra, which were continuum-fitted and normalized, and a wavelength solution was applied following the standard IRAF echelle reduction routines.

EWs were measured mainly by the direct integration of each line profile using the SPLOT task in the IRAF ECHELLE package. We estimate our measurement error in EW to be $\pm$2 mÅ from the size of noise features in the spectra and our ability to determine the proper continuum level. The EWs for our program stars are listed in Table 2.

Gratton & Ortolani (1989) and Minniti et al. (1993) obtained a spectrum of one star in common with our program stars. They used the identifications from Harris (1975), while we have used those of Walker (1994). Comparing the two shows that star I-260 from Harris (1975) is the same as the 160 from Walker (1994). Figure 3 compares EW measurements of our work with those measured by Gratton & Ortolani (1989; *crosses*) and Minniti et al. (1993; *circles*). The agreement with the latter study is quite good, with a mean difference of 2.3 $\pm$ 1.5 mÅ (in the sense of their study minus ours). The instrumental resolving powers for the two studies were very similar (27,000 vs. 28,000). However, the lower resolving power of the observations reported by Gratton & Ortolani (1989), about 15,000, appears to have led to systematically larger EWs, as Figure 3 reveals. The mean difference is 13.8 $\pm$ 2.7 mÅ.

[6] The Image Reduction and Analysis Facility is distributed by NOAO, which is operated by AURA, Inc., under contract with the NSF.

3. ANALYSIS

In our elemental abundance analysis, we use the usual spectroscopic notations that $[A/B] \equiv \log(N_A/N_B)_{\rm star} - \log(N_A/N_B)_\odot$ and that $\log n(A) \equiv \log(N_A/N_{\rm H}) + 12.00$ for each element. For the absolute solar iron abundance, we adopt $\log n({\rm Fe}) = 7.52$, following the discussion of Sneden et al. (1991).

3.1. *Line Selection and Oscillator Strengths*

For our line selection, laboratory oscillator strengths were adopted whenever possible, with supplemental solar oscillator strength values. In addition to oscillator strengths, taking into account the damping broadening due to the van der Waals force, we adopted the Unsöld approximation with no enhancement.

The abundance analysis depends mainly on the reliability of the oscillator strength values of the Fe I and Fe II lines, since not only the metallicity scale but also the stellar parameters, including the spectroscopic temperature, surface gravity, and microturbulent velocity, are determined using these lines. As discussed by Lee & Carney (2002), we mainly relied upon the extensive laboratory oscillator strength measurements by the Oxford group (Blackwell et al. 1982b, 1982c, 1986a). We also used oscillator strength values measured by O'Brian et al. (1991) and the Hannover group (Bard et al. 1991; Bard & Kock 1994). In our iron abundance analysis, we consider the Oxford group's measurements (the absorption method) as the "primary" oscillator strengths and oscillator strength measurements that relied on emission methods (O'Brian et al. 1991; Bard et al. 1991; Bard & Kock 1994) as "secondary." Therefore, the oscillator strengths by O'Brian et al. and the Hannover group were scaled with respect to those by the Oxford group as a function of excitation potential (A. A. de Almeida 2000, private communication):

$$\begin{aligned} \log gf &= \log gf({\rm OB}) - 0.017, \\ \log gf &= \log gf({\rm H91}) - 0.015 - 0.009\chi, \\ \log gf &= \log gf({\rm H94}) - 0.027 - 0.009\chi, \end{aligned} \quad (1)$$

where the excitation potential χ is given in electron volts. Blackwell et al. (1995) also pointed out that there appears to exist a slight gradient in the excitation potential between oscillator strengths by the Oxford group and those by the Hannover group, with $\log gf({\rm Oxford}) = \log gf({\rm Hannover}) - 0.021{-}0.006\chi$.

TABLE 2

Equivalent Widths

λ (Å)	Element	χ (eV)	log gf	93	117	160	89	412	350	48	Ref.[a]
6300.23	[O I]	0.000	−9.750	29	40	22	43	27	30	...	1
6363.88	[O I]	0.020	−10.250	...	8	8	9	...	...	...	1
5682.63	Na I	2.102	−0.700	24	...	5	...	13	...	19	2
5688.22	Na I	2.100	−0.460	44	13	9	8	26	31	...	2
6160.75	Na I	2.104	−1.260	11	...	...	...	6	8	...	3
5528.42	Mg I	4.350	−0.360	92	110	115	115	105	89	101	4
5711.10	Mg I	4.340	−1.630	23	37	42	40	25	...	25	4
6696.03	Al I	3.140	−1.570	16	...	...	...	8	11	...	5
6698.67	Al I	3.140	−1.890	7	...	...	...	5	4	...	5
5665.56	Si I	4.920	−2.040	7	7	7	...	7	...	...	6
5793.08	Si I	4.930	−2.060	7	8	...	...	...	6	...	6
6243.82	Si I	5.616	−1.270	5	...	...	...	6	...	...	4
6244.48	Si I	5.616	−1.270	...	...	...	...	5	...	...	4
5590.11	Ca I	2.521	−0.710	32	34	37	...	28	27	20	4
5594.46	Ca I	2.523	0.097	78	78	78	...	73	61		7
6161.30	Ca I	2.523	−1.266	15	15	15	15	12	8	...	7
6166.44	Ca I	2.521	−1.142	18	15	17	16	14	10	...	7
6169.04	Ca I	2.523	−0.797	31	27	33	33	29	25	19	7
6169.56	Ca I	2.526	−0.478	45	41	49	...	40	33	36	7
6455.60	Ca I	2.523	−1.290	...	12	13	13	...	...	...	7
6471.66	Ca I	2.526	−0.686	43	35	37	52	...	32	23	7
6499.65	Ca I	2.523	−0.818	32	28	34	39	27	24	...	7
7148.15	Ca I	2.709	0.137	85	82	86	89	...	62	65	7
5526.79	Sc I	1.768	−0.256	75	75	79	77	73	62	62	12
5657.90	Sc I	1.507	−0.645	69	76	67	71	63	64	62	12
6245.64	Sc I	1.507	−1.134	37	35	...	41	37	27	23	12
6604.60	Sc I	1.357	−1.309	36	33	33	31	29	24	22	12
5866.45	Ti I	1.067	−0.784	28	23	37	31	21	16	15	8
5899.30	Ti I	1.053	−1.098	15	13	...	17	14	...	...	8
5922.11	Ti I	1.046	−1.410	11	11	15	11	...	6	...	9
5953.16	Ti I	1.887	−0.273	10	...	15	...	...	...	...	10
5965.83	Ti I	1.879	−0.353	7	...	...	10	...	...	...	10
5978.54	Ti I	1.870	−0.500	...	8	9	...	...	...	...	4
6126.22	Ti I	1.067	−1.369	...	...	...	10	8	...	...	9
6258.11	Ti I	1.440	−0.299	27	25	34	34	21	16	13	10
6258.71	Ti I	1.460	−0.270	35	25	40	36	24	20	15	10
6261.11	Ti I	1.430	−0.423	26	20	30	29	19	15	10	10
6606.95	Ti II	2.061	−2.790	5	8	8	5	5	4	...	11
7214.74	Ti II	2.590	−1.740	11	14	13	10	12	10	...	11
6021.79	Mn I	3.080	0.030	21	22	22	21	17	16	10	12
5662.51	Fe I	4.178	−0.590	26	28	26	30	22	21	15	16
5701.55	Fe I	2.559	−2.216	56	52	57	55	49	41	39	14
5753.12	Fe I	4.260	−0.705	17	...	17	17	16	14	13	16
5816.37	Fe I	4.549	−0.618	10	...	...	10	...	...	...	16
5916.25	Fe I	2.453	−2.994	24	21	28	24	23	...	10	13
5956.69	Fe I	0.859	−4.608	64	58	...	69	50	...	...	15
6027.05	Fe I	4.076	−1.106	13	...	13	14	11	11	...	16
6065.48	Fe I	2.609	−1.530	97	88	102	96	85	75	77	14
6082.71	Fe I	2.223	−3.573	...	13	17	17	13	...	...	13
6151.62	Fe I	2.176	−3.299	28	26	33	31	23	21	17	13
6173.34	Fe I	2.223	−2.880	48	...	53	44	40	35	32	13
6180.20	Fe I	2.728	−2.637	23	...	...	21	...	...	11	18
6200.31	Fe I	2.609	−2.437	42	40	45	42	37	30	28	14
6219.28	Fe I	2.198	−2.433	84	74	84	82	67	65	50	13
6229.23	Fe I	2.845	−2.846	...	...	13	12	...	10	...	17
6230.73	Fe I	2.559	−1.281	126	114	120	122	111	102	95	14
6232.64	Fe I	3.654	−1.283	27	28	29	28	23	...	17	18
6246.32	Fe I	3.603	−0.894	52	53	58	54	52	41	35	16
6252.55	Fe I	2.404	−1.687	108	100	112	109	102	90	83	13
6265.13	Fe I	2.176	−2.550	79	68	83	81	66	64	54	13
6270.22	Fe I	2.858	−2.505	...	19	...	20	16	...	...	17
6322.69	Fe I	2.588	−2.426	41	45	51	45	41	36	28	14
6335.33	Fe I	2.198	−2.194	91	87	...	99	81	77	67	16
6336.82	Fe I	3.686	−0.916	...	41	...	...	...	...	...	18

TABLE 2—*Continued*

λ (Å)	Element	χ (eV)	log *gf*	93	117	160	89	412	350	48	Ref.[a]
6344.15	Fe I	2.433	−2.923	33	27	36	36	28	24	18	13
6393.60	Fe I	2.433	−1.469	117	108	118	116	105	99	92	17
6408.02	Fe I	3.686	−1.066	35	34	40	41	29	31	23	17
6411.65	Fe I	3.654	−0.734	59	59	65	61	54	43	42	16
6421.35	Fe I	2.280	−2.027	104	100	110	106	94	81	79	13
6430.84	Fe I	2.176	−2.006	107	108	115	114	109	92	78	13
6481.87	Fe I	2.279	−2.984	47	42	52	...	41	...	...	13
6494.98	Fe I	2.404	−1.273	142	136	131	140	128	...	107	13
6498.94	Fe I	0.958	−4.687	52	42	62	49	37	36	26	15
6574.23	Fe I	0.990	−5.004	25	26	36	34	26	17	13	15
6575.02	Fe I	2.588	−2.727	27	29	33	32	27	23	13	16
6581.21	Fe I	1.485	−4.707	13	...	17	14	...	...	...	17
6592.91	Fe I	2.728	−1.490	98	88	96	94	87	79	68	16
6593.87	Fe I	2.433	−2.422	67	55	65	69	56	50	38	13
6609.11	Fe I	2.559	−2.692	32	35	38	36	33	24	16	14
6625.02	Fe I	1.011	−5.366	13	...	19	14	12	9	...	15
6663.44	Fe I	2.420	−2.479	62	62	70	64	54	47	41	13
6677.99	Fe I	2.692	−1.435	105	104	109	103	98	89	77	16
6750.15	Fe I	2.424	−2.621	51	50	62	60	50	42	34	13
6978.85	Fe I	2.484	−2.500	57	48	67	58	51	41	35	13
7223.66	Fe I	3.017	−2.269	25	25	28	27	24	18	...	18
7511.01	Fe I	4.178	0.082	75	70	74	74	64	59	50	16
7710.36	Fe I	4.220	−1.129	...	...	13	...	...	...	...	16
7723.20	Fe I	2.279	−3.617	18	...	20	14	13	...	...	13
5991.38	Fe II	3.153	−3.557	...	12	...	...	...	...	...	19
6149.26	Fe II	3.889	−2.724	10	12	...	10	...	...	...	19
6247.56	Fe II	3.891	−2.329	...	...	21	25	19	20	19	19
6416.92	Fe II	3.891	−2.740	...	12	...	...	...	...	...	19
6432.68	Fe II	2.891	−3.708	20	22	19	21	19	18	15	19
6456.38	Fe II	3.903	−2.075	33	32	29	31	32	31	24	19
6176.81	Ni I	4.088	−0.530	6	...	...	...	...	...	...	20
6586.31	Ni I	1.951	−2.810	15	10	22	18	14	8	...	20
6643.63	Ni I	1.676	−2.010	80	67	87	80	70	55	55	4
6767.77	Ni I	1.826	−2.170	71	57	74	66	58	44	34	20
5782.13	Cu I	1.642	−1.700	11	...	11	9	...	6	...	21
5853.69	Ba II	0.600	−1.010	72	56	69	74	65	62	63	5
6141.73	Ba II	0.700	−0.080	131	109	120	113	117	113	103	5
6496.91	Ba II	0.600	−0.380	127	109	119	122	119	113	98	5
6390.48	La II	0.321	−1.410	5	...	5	...	6	...	...	4
6774.27	La II	0.126	−1.750	7	...	...	...	6	...	...	4
6645.06	Eu II	1.380	0.204	6	5	8	9	7	10	...	22
7217.55	Eu II	1.230	−0.301	3	...	7	8	...	...	...	22
7426.57	Eu II	1.279	−0.149	5	...	...	...	...	...	...	22

[a] See Table 3.

For neutral titanium lines, we relied on the laboratory measurements by the Oxford group (Blackwell et al. 1982a, 1983, 1986b). It should be noted that the original Oxford *gf*-values have been increased by +0.056 dex following Grevesse et al. (1989). They pointed out that the Oxford *gf*-values relied on inaccurate lifetime measurements and that the absolute *gf*-values should be revised on the basis of the new measurements.

Hyperfine splitting (HFS) components must be considered in the barium abundance analysis because Ba II lines are usually very strong even in metal-poor stars and the desaturation effects due to HFS components become evident (see, for example, McWilliam 1998). We adopted the Ba II HFS components and oscillator strengths of Sneden et al. (1997). We also perform HFS treatment for scandium, manganese (Prochaska & McWilliam 2000), and copper (Kurucz 1993). For the copper HFS analysis, we adopt the solar Cu isotopic ratio, 69% ^{63}Cu and 31% ^{65}Cu, following the discussions given by Smith et al. (2000) and Simmerer et al. (2003). The EWs of Mn I λ6021.79 and Cu I λ5782.13 lines in our program stars are weak, and the Mn and Cu abundance differences between HFS treatment and non-HFS treatment are no larger than 0.02 dex. We list our source of oscillator strengths for each element in Table 3.

3.2. *Stellar Parameters and Model Atmospheres*

Having good stellar parameters, such as the effective temperature and the surface gravity, is critical for any stellar abundance study, since the absolute or the relative elemental abundance scale will depend on the input stellar parameters. For our analysis, we rely on spectroscopic temperatures and photometric surface gravities, following the method described in Lee & Carney (2002; see also Ivans et al. 2001, Kraft & Ivans 2003, and Sneden et al. 2004). It has been suspected by others that the traditional spectroscopic surface gravity determination method, which requires the same elemental abundances derived

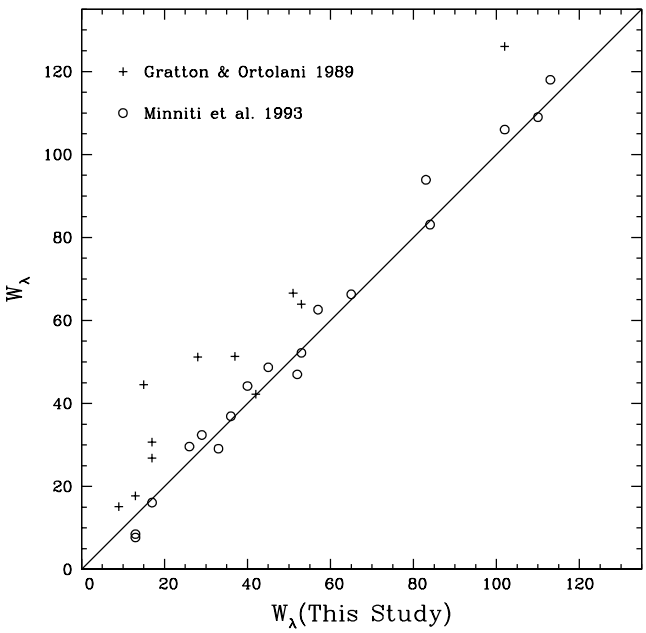

FIG. 3.—Comparison of EWs of the star 160 with those of Gratton & Ortolani (1989) and Minniti et al. (1993).

from neutral and singly ionized lines (preferentially Fe I and Fe II lines), suffers from non-LTE (NLTE) effects (see, for example, Nissen et al. 1997 and Allende Prieto et al. 1999). Since metal-poor stars have much weaker metal absorption in the ultraviolet, more nonlocal UV flux can penetrate from the deeper layers. This flux is vital in determining the ionization equilibrium of the atoms, resulting in deviations from local thermodynamic equilibrium (LTE). Nissen et al. (1997) claimed that surface gravities of metal-poor dwarfs and subgiants derived from the spectroscopic method, which requires the Fe I and Fe II lines to provide the same iron abundance, are a factor of 2 or 3 ($\Delta \log g \approx 0.3$–$0.5$) smaller than those from the *Hipparcos* parallaxes. Allende Prieto et al. (1999) also claimed that spectroscopic gravities and those from the *Hipparcos* parallaxes are in good agreement for stars in the metallicity range $-1.0 < [\mathrm{Fe/H}] < +0.3$, while large discrepancies can be found for stars with metallicities below $[\mathrm{Fe/H}] = -1.0$, in the sense that the spectroscopic method provides lower surface gravities. Therefore, we rely on photometric gravities for our abundance analysis.

The initial estimates of the temperature of program stars were estimated using the *BVK* photometry of our program stars (Cutri et al. 2000; Frogel et al. 1983; Walker 1994) and the empirical color-temperature relations given by Alonso et al. (1999). Since their relation depends slightly on the metallicity, we adopted $[\mathrm{Fe/H}] = -2.1$ for M68 (Harris 1996). To estimate the dereddened color, we adopted $E(B-V) = 0.07$ (Walker 1994). Note that Alonso et al. (1999) employed the Carlos Sánchez Telescope (TCS) system for their infrared color-temperature relations and we used the relation given by Alonso et al. (1998) to convert the CIT system to the TCS system for the K magnitudes listed in Table 1. To derive photometric surface gravity in relation to that of the Sun, we use $\log g_\odot = 4.44$ in cgs units, $M_{\mathrm{bol},\odot} = 4.74$ mag, and $T_{\mathrm{eff},\odot} = 5777$ K for the Sun (Livingston 1999), and we assume the stellar masses for all the red giants stars in this analysis to be $M = 0.8\ M_\odot$. We use the empirical relation given by Alonso et al. (1999) to estimate the bolometric correction, and we adopt $(m-M)_0 = 14.97$ mag for the cluster (Harris 1996).

With initial photometric temperature and surface gravity estimates, 72 depth plane–parallel LTE model atmospheres were computed using the program ATLAS9, written and supplied by R. L. Kurucz. Assuming that all of the cluster's stars would prove to be metal-poor, the model atmospheres were computed using opacity distribution functions and abundances with all the α-elements (O, Ne, Mg, Si, S, Ar, Ca, and Ti) enhanced by 0.4 dex. The α-element enhancements are important, since several of these elements are quite abundant and are major electron donors to the H^- opacity. During our model computation, convective overshoot was turned off.

The abundance analysis was performed using the current version (2002) of the LTE line analysis program MOOG (Sneden 1973). Adopting the photometric temperature and

TABLE 3
REFERENCES FOR $\log gf$-VALUES

Ref. No.	Reference	Element
1	Lambert (1978)	[O I]
2	Ivans et al. (2001)	Na I
3	Kraft et al. (1992)	Na I
4	Sneden et al. (2004)	Mg I, Si I, Ca I, Ti I, Ni I, La II
5	Sneden et al. (1997)	Al I, Ba II
6	Garz (1973)	Si I
7	Smith (1981)	Ca I
8	Blackwell et al. (1982a)	Ti I
9	Blackwell et al. (1983)	Ti I
10	Blackwell et al. (1986b)	Ti I
11	Fuhr et al. (1988a)	Ti II
12	Prochaska & McWilliam (2000)	Sc I, Mn I
13	Blackwell et al. (1982b)	Fe I
14	Blackwell et al. (1982c)	Fe I
15	Blackwell et al. (1986a)	Fe I
16	O'Brian et al. (1991)	Fe I
17	Bard et al. (1991)	Fe I
18	Bard & Kock (1994)	Fe I
19	Biémont et al. (1991)	Fe II
20	Fuhr et al. (1988b)	Ni I
21	Kurucz (1993)	Cu I
22	Biémont et al. (1982)	Eu II

TABLE 4
Model Atmosphere Parameters

Star (1)	$T_{\rm eff}$ (K) $(B-V)$[a] (2)	$(V-K)$[a] (FPC83) (3)	$(V-K)$[a] (2MASS) (4)	(FPC83)[b] (5)	(spec) (6)	log g (phot) (7)	log g (spec) (8)	$v_{\rm turb}$ (km s^{-1}) (9)
93	4220	4215	4240	4287	4200	0.7	0.1	1.95
117	4370	4340	4335	4501	4300	0.8	0.3	1.80
160	4200	4200	4200	4329	4100	0.7	0.0	1.80
89	4200	4200	4215	4279	4175	0.7	0.0	1.90
412	4275	4290	4300	4372	4200	0.8	0.1	1.75
350	4390	...	4340	...	4300	1.0	0.3	1.60
48	4450	...	4450	...	4325	1.1	0.3	1.75

[a] Using relations given by Alonso et al. (1999).
[b] Frogel et al. (1983).

surface gravity as our initial values, we began by restricting the analysis to those Fe I lines with log $(W_\lambda/\lambda) \leq -5.2$ (i.e., for the linear part of the curve of growth) and comparing the abundances as a function of excitation potential. New model atmospheres were computed with a slightly different effective temperature until the slope of the log n(Fe I) versus excitation potential relation was zero to within the uncertainties. The stronger Fe I lines were then added and the microturbulent velocity $v_{\rm turb}$ altered until the log n(Fe I) versus log (W_λ/λ) relation had no discernible slope.

Table 4 shows our temperature and surface gravity of program stars. In the fifth column of the table, we also show the temperature of five stars in common given by Frogel et al. (1983). Please note that Gratton & Ortolani relied on temperatures given by Frogel et al. (1983), which are 159 ± 27 K higher than our spectroscopic temperatures. The temperature difference between those derived from $B-V$ colors (col. [2]) and spectroscopic temperatures of this study is 72 ± 15 K (seven stars), in the sense that our spectroscopic temperature is low. The temperature difference between those derived from $V-K$ colors using K magnitudes of Frogel et al. (col. [3]) and spectroscopic temperatures of this study is 54 ± 17 K (five stars), and those derived from $V-K$ colors using 2MASS K magnitudes (col. [4]) and spectroscopic temperatures of this study are 69 ± 14 K (seven stars). The discrepancy between the photometric and spectroscopic temperatures from $V-K$ colors is slightly smaller than that from $B-V$ colors.

4. RESULTS

4.1. *Elemental Abundances and Error Analysis*

In Table 5, we present the elemental abundances of our program stars using photometric surface gravities and spectroscopic temperatures. The [el/Fe] ratios for neutral elements are estimated from [el/H] and [Fe I/H] ratios, with the exception of oxygen. The [el/Fe] for singly ionized elements (Ti II, Ba II, La II, and Eu II) and oxygen are estimated from [el/H] and [Fe II/H] ratios (see, for example, Ivans et al. 2001, Kraft & Ivans 2003, and Sneden et al. 2004). The internal uncertainty quoted is for a single line, and therefore, that of each element is given by $\sigma/\sqrt{n}$, where σ is the uncertainty per line and n is the number of absorption lines used for each element. Systematic errors, such as in adopted gf-values as a function of excitation potential, which could lead to systematically erroneous temperature estimates, are not included. The last two columns of the table show the mean values of each element of the cluster with and without star 117 (ZNG2), an ultraviolet-bright, post-AGB star according to Zinn et al. (1972). We adopt iron abundances on the basis of only the Fe II lines for our program stars, since the Fe II abundance is thought to be less sensitive to NLTE conditions (see, for example, Thévenin & Idiart 1999 and Kraft & Ivans 2003). In Figure 4, we show abundances of all elements measured in this study against $T_{\rm eff}$, showing no discernible gradient in elemental abundances with $T_{\rm eff}$. The mean [Fe/H] of −2.16 dex for our seven stars is measured with a small internal uncertainty of ±0.02 ($\sigma = 0.04$).

For comparison, we also show the elemental abundances of our program stars using the traditional spectroscopic surface gravities in Table 6 (see col. [7] of Table 4). In the table, the [el/Fe] ratios are derived from [el/H] and mean [Fe/H] ratios. In Table 7, we show differences in elemental abundances using photometric and spectroscopic gravities. The [Fe/H] ratio using spectroscopic gravities is 0.25 dex lower than that using photometric gravities. For other elements, however, the elemental abundances from two different methods are in good agreement to within 0.10 dex. Therefore, these small differences suggest that we are still able, in principle, to compare our elemental abundances with other results using the different surface gravity determination method. Nonetheless, we reiterate that we choose to employ photometric gravities and discuss only the results from Table 5.

In Table 8, we show estimated errors resulting from uncertainties in the input model atmosphere $\delta T_{\rm eff} = \pm 80$ K, $\delta \log g = \pm 0.3$, and $\delta v_{\rm turb} = \pm 0.2$ km s^{-1}, which are appropriate for our analysis. The Fe, Si, Ba, and La abundances are sensitive to $T_{\rm eff}$, resulting in $|\delta[{\rm el/Fe\ (or\ H\ for\ Fe)}]/\delta T_{\rm eff}(80\ {\rm K})| \approx 0.08$–0.12 dex. The iron abundance from Fe II lines is sensitive to surface gravity, $|\delta[{\rm Fe\ II/H}]/\delta \log g(0.3\ {\rm dex})| \approx 0.10$ dex. Since our program stars are metal-poor, absorption lines are usually weak, as listed in Table 2. Therefore, our derived elemental abundances are less sensitive to microturbulent velocity. The barium abundance is the most sensitive to microturbulent velocity, resulting in $|\delta[{\rm Ba/Fe}]/\delta v_{\rm turb}(0.2\ {\rm km\ s^{-1}})| \approx 0.09$ dex.

4.2. *Comparisons with Previous Results*

As mentioned above, Gratton & Ortolani (1989) and Minniti et al. (1993, 1996) derived abundances for star 160 (I-260 from Harris 1975). In Table 9, we compare our stellar parameters and elemental abundances of this star with those of Gratton & Ortolani (1989) and Minniti et al. (1993, 1996).

TABLE 5

Elemental Abundances of M68 with Photometric log g

Abundance	93	117	160	89	412	350	48	Mean	Mean[a]
$[Fe/H]_{I}$	−2.50	−2.38	−2.56	−2.51	−2.58	−2.53	−2.67	−2.53	−2.56
n	43	38	42	45	42	35	35	7	6
σ	0.05	0.06	0.05	0.05	0.06	0.05	0.06	0.09	0.06
$[Fe/H]_{II}$	−2.17	−2.16	−2.12	−2.14	−2.16	−2.15	−2.23	−2.16	−2.16
n	3	5	3	4	3	3	3	7	6
σ	0.03	0.05	0.02	0.06	0.05	0.02	0.06	0.03	0.04
[O/Fe]	+0.37	+0.46	+0.23	+0.43	+0.37	+0.51	+0.59	+0.42	+0.42
n	1	2	2	2	1	1	2	7	6
σ	...	0.20	0.01	0.20	...	...	0.05	0.12	0.13
[Na/Fe]	+0.62	−0.07	−0.23	−0.27	+0.38	+0.55	+0.39	+0.23	+0.24
n	3	1	2	1	3	2	1	7	6
σ	0.07	...	0.00	...	0.08	0.05	...	0.40	0.39
[Mg/Fe]	+0.12	+0.39	+0.50	+0.47	+0.35	+0.19	+0.45	+0.35	+0.35
n	2	2	2	2	2	1	2	7	6
σ	0.05	0.01	0.01	0.01	0.10	...	0.03	0.14	0.16
[Al/Fe]	+1.18	...	...	...	+1.00	+1.07	...	+1.08	+1.08
n	2	...	...	...	2	2	...	3	3
σ	0.05	...	...	...	0.07	0.07	...	0.09	0.09
[Si/Fe]	+0.68	+0.65	+0.77	...	+0.75	+0.72	...	+0.71	+0.73
n	3	2	1	...	3	1	...	5	4
σ	0.05	0.04	...	...	0.05	...	...	0.05	0.04
[Ca/Fe]	+0.33	+0.27	+0.29	+0.37	+0.30	+0.23	+0.32	+0.30	+0.31
n	9	10	10	7	7	9	5	7	6
σ	0.05	0.07	0.04	0.08	0.04	0.07	0.05	0.04	0.05
$[Sc/Fe]_{II}$	+0.14	+0.19	+0.16	+0.14	+0.13	+0.07	+0.13	+0.14	+0.13
n	4	4	3	4	4	4	4	7	6
σ	0.14	0.20	0.25	0.20	0.18	0.18	0.18	0.04	0.03
$[Ti/Fe]_{I}$	+0.06	+0.07	+0.09	+0.03	−0.02	−0.02	+0.01	+0.03	+0.02
n	8	6	7	8	6	5	4	7	6
σ	0.07	0.05	0.07	0.05	0.04	0.06	0.05	0.04	0.05
$[Ti/Fe]_{II}$	−0.12	+0.09	+0.01	−0.15	−0.06	−0.08	...	−0.05	−0.08
n	2	2	2	2	2	2	...	6	5
σ	0.03	0.12	0.08	0.05	0.01	0.02	...	0.09	0.06
$[Ti/Fe]_{mean}$	−0.03	+0.08	+0.05	−0.06	−0.04	−0.05	+0.01	−0.01	−0.03
[Mn/Fe]	−0.25	−0.22	−0.30	−0.27	−0.29	−0.26	−0.33	−0.27	−0.28
n	1	1	1	1	1	1	1	7	6
σ	...	...	...	...	...	...	...	0.04	0.03
[Ni/Fe]	−0.04	−0.21	−0.01	−0.09	−0.09	−0.22	−0.14	−0.11	−0.10
n	4	3	3	3	3	3	2	7	6
σ	0.11	0.11	0.08	0.09	0.09	0.09	0.00	0.08	0.07
[Cu/Fe]	−0.74	...	−0.83	−0.86	...	−0.85	...	−0.82	−0.82
n	1	...	1	1	...	1	...	4	4
σ	...	...	...	...	...	...	...	0.05	0.05
$[Ba/Fe]_{II}$	−0.28	−0.46	−0.39	−0.40	−0.30	−0.19	−0.32	−0.33	−0.31
n	3	3	3	3	3	3	3	7	6
σ	0.09	0.12	0.06	0.10	0.12	0.14	0.04	0.09	0.08
$[La/Fe]_{II}$	−0.23	...	−0.40	...	−0.19	...	...	−0.27	−0.27
n	2	...	1	...	2	...	...	3	3
σ	0.14	...	...	...	0.03	...	...	0.11	0.11
$[Eu/Fe]_{II}$	+0.06	+0.01	+0.18	+0.28	+0.11	+0.37	...	+0.17	+0.20
n	3	1	2	2	1	1	...	6	5
σ	0.08	...	0.13	0.12	...	...	...	0.14	0.13

[a] Without the star 117.

Gratton & Ortolani (1989) relied on the results from Frogel et al. (1983) for the estimated temperature and surface gravity. Table 4 shows that this results in a $T_{\rm eff}$ estimate 230 K hotter than our spectroscopic measurement, as well as a slightly lower microturbulent velocity (by 0.2 km s^{-1}). Our results suggest that a difference in microturbulent velocity of 0.2 km s^{-1} does not alter the derived iron abundances and element-to-iron ratios by more than about 0.1 dex. As discussed above (see also Fig. 3), the EWs measured by Gratton & Ortolani are about 14 mÅ larger than our measurements. This was also noticed by Minniti et al. (1993), who found a difference in EW of 10.2 ± 9.0 mÅ, in the sense of Gratton & Ortolani minus Minniti et al. Therefore, the larger EWs with the warmer surface temperature are the probable cause of the higher [Fe/H]-value they derived. Therefore, the detailed comparison of each elemental abundance between this study and Gratton & Ortolani may not be meaningful.

TABLE 6

Elemental Abundances of M68 with Spectroscopic log g

Abundance	93	117	160	89	412	350	48	Mean	Mean[a]
$[Fe/H]_{I}$	−2.40	−2.30	−2.46	−2.40	−2.47	−2.43	−2.56	−2.43	−2.45
n	43	38	42	45	42	35	35	7	6
σ	0.05	0.06	0.05	0.06	0.06	0.05	0.07	0.08	0.06
$[Fe/H]_{II}$	−2.37	−2.33	−2.35	−2.36	−2.39	−2.39	−2.52	−2.39	−2.40
n	3	5	3	4	3	3	3	7	6
σ	0.02	0.05	0.02	0.06	0.04	0.02	0.06	0.06	0.06
$[Fe/H]_{mean}$	−2.39	−2.32	−2.41	−2.38	−2.43	−2.41	−2.54	−2.43	−2.41
[O/Fe]	+0.38	+0.43	+0.23	+0.42	+0.39	+0.51	+0.60	+0.42	+0.42
n	1	2	2	2	1	1	2	7	6
σ	...	0.20	0.01	0.21	...	...	0.06	0.11	0.13
[Na/Fe]	+0.65	−0.04	−0.21	−0.24	+0.38	+0.56	+0.40	+0.21	+0.26
n	3	1	2	1	3	2	1	7	6
σ	0.08	...	0.00	...	0.07	0.05	...	0.37	0.39
[Mg/Fe]	+0.19	+0.48	+0.60	+0.60	+0.43	+0.32	+0.53	+0.45	+0.45
n	2	2	2	2	2	1	2	7	6
σ	0.03	0.06	0.08	0.08	0.21	...	0.13	0.15	0.17
[Al/Fe]	+1.16	...	...	...	+0.98	+1.04	...	+1.06	+1.06
n	2	...	...	...	2	2	...	3	3
σ	0.06	...	...	...	0.07	0.07	...	0.09	0.09
[Si/Fe]	+0.62	+0.63	+0.67	...	+0.66	+0.64	...	+0.64	+0.65
n	3	2	1	...	3	1	...	5	4
σ	0.06	0.04	...	...	0.06	...	...	0.02	0.02
[Ca/Fe]	+0.36	+0.31	+0.31	+0.39	+0.31	+0.24	+0.32	+0.32	+0.32
n	9	10	10	7	7	9	5	7	6
σ	0.04	0.08	0.07	0.09	0.06	0.07	0.05	0.05	0.05
$[Sc/Fe]_{II}$	+0.23	+0.22	+0.33	+0.23	+0.24	+0.14	+0.20	+0.23	+0.23
n	4	4	3	4	4	4	4	7	6
σ	0.19	0.22	0.34	0.26	0.24	0.22	0.22	0.06	0.06
$[Ti/Fe]_{I}$	+0.06	+0.08	+0.06	+0.08	−0.04	−0.02	+0.01	+0.03	+0.03
n	8	6	7	8	6	5	4	7	6
σ	0.07	0.05	0.09	0.06	0.04	0.06	0.06	0.05	0.05
$[Ti/Fe]_{II}$	−0.10	+0.08	+0.06	−0.15	−0.02	−0.06	...	−0.03	−0.05
n	2	2	2	2	2	2	...	6	5
σ	0.02	0.13	0.10	0.06	0.00	0.03	...	0.09	0.08
$[Ti/Fe]_{mean}$	−0.02	+0.08	+0.06	−0.04	−0.03	−0.04	+0.01	+0.00	−0.01
[Mn/Fe]	−0.24	−0.19	−0.31	−0.25	−0.30	−0.26	−0.33	−0.27	−0.28
n	1	1	1	1	1	1	1	7	6
σ	...	...	...	...	...	...	...	0.05	0.04
[Ni/Fe]	−0.04	−0.22	−0.13	−0.16	−0.18	−0.27	−0.19	−0.17	−0.16
n	4	3	3	3	3	3	2	7	6
σ	0.11	0.11	0.09	0.09	0.09	0.09	0.00	0.07	0.08
[Cu/Fe]	−0.76	...	−0.90	−0.88	...	−0.87	...	−0.86	−0.86
n	1	...	1	1	...	1	...	4	4
σ	...	...	...	...	...	...	...	0.06	0.06
$[Ba/Fe]_{II}$	−0.18	−0.44	−0.24	−0.31	−0.18	−0.12	−0.24	−0.24	−0.21
n	3	3	3	3	3	3	3	7	6
σ	0.11	0.11	0.05	0.10	0.12	0.13	0.06	0.11	0.07
$[La/Fe]_{II}$	−0.20	...	−0.33	...	−0.15	...	...	−0.23	−0.23
n	2	...	1	...	2	...	...	3	3
σ	0.13	...	...	...	0.02	...	...	0.10	0.10
$[Eu/Fe]_{II}$	+0.06	+0.01	+0.24	+0.28	+0.15	+0.39	...	+0.18	+0.22
n	3	1	2	2	1	1	...	6	5
σ	0.08	...	0.12	0.11	...	...	...	0.14	0.13

[a] Without the star 117.

Minniti et al. (1993) derived an even higher temperature of the star, $T_{eff} = 4400$ K, which is 300 K warmer than our temperature, and consequently their iron abundance of the star from Fe I lines is about 0.45 dex higher than our value, although, interestingly, very close to the value we obtain using only the Fe II lines. Minniti et al. (1993) obtained $\log g = 1.0$ for the star, using the ionization equilibrium of iron lines, which is about 0.3 dex larger than those of Gratton & Ortolani (1989) and this study. This is very worrisome, since Minniti et al. (1993) used the same temperature determination method, the same model atmospheres as this study, and similar oscillator strength values. Their instrumental resolution was comparable to ours, and although they employed the program WIDTH rather than MOOG, both programs yield the same results in our experience, at least when the atomic data are identical. The EWs are also in good agreement, as noted earlier. In particular, the agreement in the

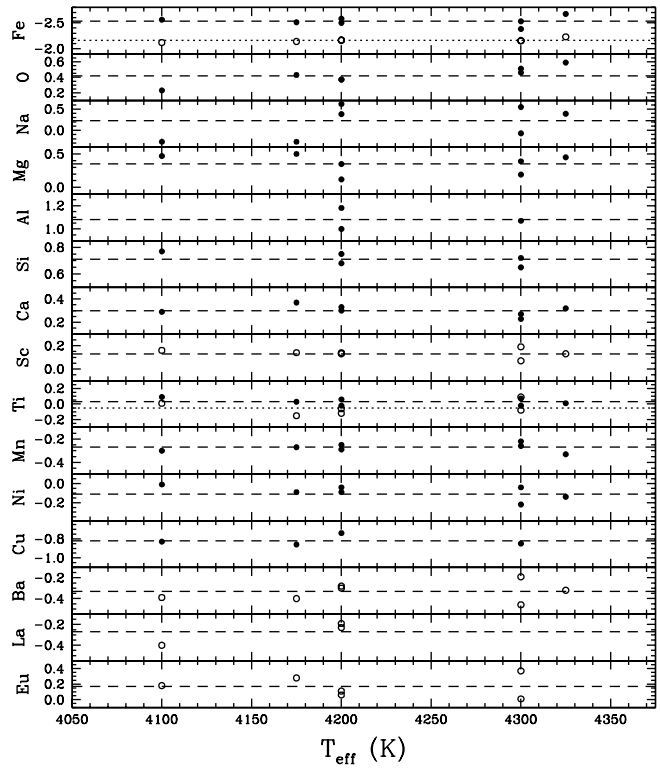

FIG. 4.—Elemental abundances studied in this work plotted against $T_{\rm eff}$. Note that the ordinate of the top panel is [Fe/H], while the ordinates of the remaining panels are [el/Fe] ratios. Neutral atoms are presented by filled circles and singly ionized atoms by open circles. Dashed lines are the mean abundances of each element. The mean Fe II and Ti II abundances are presented by dotted lines.

EWs of weak lines (i.e., the lines on the linear part of the curve of growth) appears to be excellent. For lines with $\log(W_\lambda/\lambda) \leq -5.2$, the difference in EWs is -1.7 ± 1.4 mÅ (seven lines), in the sense of Minniti et al. minus this study.

Instead of comparing our results with those of Minniti et al. (1993) directly, we have rederived the surface temperature using the EWs measured by Minniti et al. (1993). In their Table 2,[7] Minniti et al. (1993) presented Fe I and Fe II line widths of the star 160. Using their Fe I line widths with $\log(W_\lambda/\lambda) \leq -5.2$, we ran MOOG for this star again. At this time, we use a Kurucz model atmosphere with $T_{\rm eff} = 4400$ K, $\log g = 1.0$, and $v_{\rm turb} = 2.0$ km s^{-1} as our initial input model. Note that these stellar parameters are derived by Minniti et al. for their analyses of the star, as shown in Table 9. We show the results from our MOOG run in Figure 5*a*. We obtain [Fe/H] $= -2.18 \pm 0.29$ (36 lines), and this value is very similar to that of Minniti et al., [Fe/H] $= -2.11$. As can be seen in the figure, however, the scatter in our analysis using the line list of Minniti et al. is much larger than that Minniti et al. estimated ($\sigma \leq 0.07$ dex per line), and we were not able to reproduce their results using their input data. We find it necessary to adopt a different temperature. Since the Fe I line at λ6353.84 deviates far from the mean value of the relation, we excluded this line and ran MOOG again, with $T_{\rm eff} = 4275$ K, and obtained [Fe/H] $= -2.30 \pm 0.22$ dex (Fig. 5*b*). For comparison, we show the results from MOOG run with our stellar parameters, $T_{\rm eff} = 4100$ K, $\log g = 0.7$, and $v_{\rm turb} = 1.8$ km s^{-1} in Figure 5*c*. We obtain [Fe/H] $= -2.50 \pm 0.13$. In the figure, the agreement between results from our EWs and those of Minniti et al. for lines with $\chi \leq 3$ eV is good. For lines with $\chi > 3$ eV, the scatter in results from Minniti et al. is rather large. It is likely that the Fe I lines employed by Minniti et al. may have been contaminated, and as a result they would have obtained a higher iron abundance than we have. Their accidental inclusion of Fe I lines suffering from line blending made their measurements meet the ionization equilibrium at high surface gravity $\log g = 1.0$. Using our line width measurements listed in Table 2, the criterion of the ionization equilibrium of iron lines is not satisfied until the surface gravity becomes as low as $\log g = 0.0$, and this surface gravity value is not only 1 dex smaller than that of Minniti et al. but is also implausible.

We conclude that we do not understand why we cannot obtain the same results as Minniti et al. (1993) using their data, and

[7] The titles of cols. (2) and (3) in Table 2 of Minniti et al. (1993) should be switched.

TABLE 7

DIFFERENCES IN ELEMENTAL ABUNDANCES USING PHOTOMETRIC AND SPECTROSCOPIC SURFACE GRAVITIES

Element	$[{\rm el/Fe}]_{\rm phot} - [{\rm el/Fe}]_{\rm spec}$
[Fe/H]	+0.25 ± 0.05
[O/Fe]	+0.01 ± 0.01
[Na/Fe]	−0.02 ± 0.01
[Mg/Fe]	−0.10 ± 0.02
[Al/Fe]	+0.02 ± 0.01
[Si/Fe]	+0.07 ± 0.03
[Ca/Fe]	−0.02 ± 0.01
$[{\rm Sc/Fe}]_{\rm II}$	−0.09 ± 0.04
$[{\rm Ti/Fe}]_{\rm I}$	+0.00 ± 0.03
$[{\rm Ti/Fe}]_{\rm II}$	−0.02 ± 0.02
$[{\rm Ti/Fe}]_{\rm mean}$	−0.01 ± 0.01
[Mn/Fe]	−0.01 ± 0.02
[Ni/Fe]	+0.05 ± 0.04
[Cu/Fe]	+0.03 ± 0.03
$[{\rm Ba/Fe}]_{\rm II}$	−0.10 ± 0.04
$[{\rm La/Fe}]_{\rm II}$	−0.05 ± 0.02
$[{\rm Eu/Fe}]_{\rm II}$	−0.02 ± 0.03

TABLE 8

ABUNDANCE DEPENDENCES ON MODEL ATMOSPHERE

Element	$\delta T_{\rm eff}$ ±80 (K)	$\delta \log g$ ±0.3	$\delta v_{\rm turb}$ ±0.2 (km s^{-1})
$[{\rm Fe/H}]_{\rm I}$	±0.12	∓0.03	∓0.03
$[{\rm Fe/H}]_{\rm II}$	∓0.06	±0.10	±0.02
[O/Fe]	±0.04	±0.05	∓0.03
[Na/Fe]	±0.03	∓0.03	±0.03
[Mg/Fe]	∓0.05	∓0.05	±0.01
[Al/Fe]	∓0.06	∓0.01	±0.03
[Si/Fe]	∓0.10	±0.01	±0.04
[Ca/Fe]	∓0.04	∓0.04	±0.01
$[{\rm Sc/Fe}]_{\rm II}$	±0.06	∓0.02	∓0.01
$[{\rm Ti/Fe}]_{\rm I}$	±0.03	∓0.02	±0.03
$[{\rm Ti/Fe}]_{\rm II}$	±0.04	±0.00	±0.02
[Mn/Fe]	∓0.02	∓0.03	±0.04
[Ni/Fe]	∓0.02	±0.01	±0.01
[Cu/Fe]	±0.01	±0.01	±0.02
$[{\rm Ba/Fe}]_{\rm II}$	±0.08	∓0.02	∓0.09
$[{\rm La/Fe}]_{\rm II}$	±0.09	∓0.01	±0.02
$[{\rm Eu/Fe}]_{\rm II}$	±0.06	±0.00	±0.02

TABLE 9
STELLAR PARAMETERS AND ELEMENTAL ABUNDANCES OF THE STAR 160

Parameter	This Study	Gratton & Ortolani (1989)	Minniti et al. (1993, 1996)
$T_{\rm eff}$ (K)	4100	4329	4400
log g	0.7	0.75	1.0
Method	Phot.	Phot.	Spec.
$v_{\rm turb}$ (km s^{-1})	1.8	1.6	2.0
[Fe/H]$_{\rm I}$	−2.56	−1.94	−2.11
[Fe/H]$_{\rm II}$	−2.17	...	−2.14
[O/Fe]	+0.23	+0.22	+0.25
[Na/Fe]	−0.23	−0.04	−0.08
[Mg/Fe]	+0.50	+0.07	...
[Si/Fe]	+0.77	+0.41	...
[Ca/Fe]	+0.29	+0.25	...
[Ti/Fe]	+0.05	+0.43	...
[Ni/Fe]	−0.01	−0.15	...
[Ba/Fe]	−0.39	−0.33	...

we conclude that the agreement between their [Fe/H] result and ours is probably fortuitous.

5. DISCUSSION

In the previous section, we discussed the rationale by which we have derived elemental abundance estimates. From the ionized iron lines, we obtain [Fe/H] $= -2.16 \pm 0.02$ ($\sigma = 0.04$) for M68 (on the basis of internal errors only). Element-to-iron ratios are matched using comparable ionization states (except for oxygen, given its very high ionization potential).

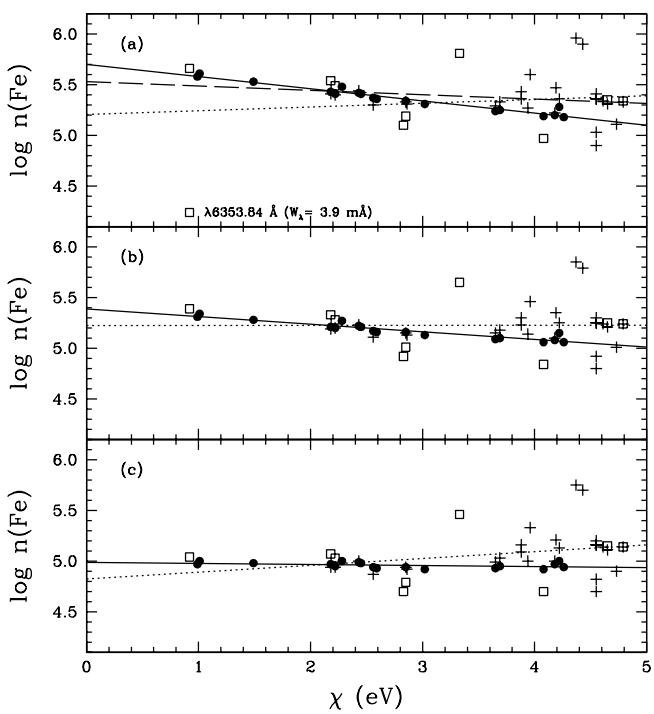

FIG. 5.—(*a*) The log n(Fe) vs. excitation potential relation of the star M68-160 (I260) using Fe I EWs of Minniti et al. (1993) with log $(W_\lambda/\lambda) \leq -5.2$ for $T_{\rm eff} = 4400$ K, log $g = 1.0$, and $v_{\rm turb} = 2.0$ km s^{-1}. Plus signs are for Fe I lines with $W_\lambda > 10$ mÅ, and open squares are for $W_\lambda \leq 10$ mÅ from Minniti et al. (1993). The dotted and the dashed lines represent the least-squares fits to the data with and without, respectively, Fe I λ6538.84. Filled circles show the relation using Fe I EWs of this study, and the solid line is for the least square fit to the data. (*b*) Same as (*a*), but using the model atmosphere with $T_{\rm eff} = 4275$ K, log $g = 1.0$, and $v_{\rm turb} = 2.0$ km s^{-1}, and the Fe I λ6538.84 line is not used. (*c*) Same as (*b*), but using the model atmosphere with $T_{\rm eff} = 4100$ K, log $g = 0.7$, and $v_{\rm turb} = 1.8$ km s^{-1}.

We explore the abundances of a variety of elements relative to iron. In the interests of economy and interest, we focus on comparisons between M68 and the comparably metal-poor globular cluster M15, on the basis of the results of Sneden et al. (1997, 2000a), and then discuss these in turn, compared with other ensembles of field stars and clusters. We select M15 partly because it is one of the few metal-poor globular clusters with comparable data for the neutron capture elements lanthanum, barium, and europium, and partly because of the hypothesized common origin (Yoon & Lee 2002).

5.1. *Mixing or Primordial Variations?* O, Na, Mg, *and* Al

Many globular clusters appear to show anticorrelations between the abundances of oxygen and sodium and of magnesium and aluminum. The subject was reviewed by Kraft (1994) and has been revisited by numerous authors. The approach often taken has been that these anticorrelations arise from deep mixing, whereby material whose chemical compositions have been altered by proton captures within the CNO cycle have been brought to the stellar surface. This concept has become less plausible with the discovery that such anticorrelations are seen in relatively unevolved stars in the metal-poor clusters NGC 6397 and NGC 6752 (Gratton et al. 2001) and in the metal-rich cluster 47 Tuc (Carretta et al. 2004). The variations seen in some of these elements in Table 5 nonetheless warrant a quick look at these possible anticorrelations in M68, and we show them here, in Figure 6, in comparison with the results for M15 from Sneden et al. (1997).

There are three relatively interesting results here. First is that M68 does show a variation, especially in sodium. The second is that the large range in sodium abundances is *not* matched by a correlated (or anticorrelated) variation in the oxygen abundances, as appears to be the case for M15. Finally, the post-AGB star 117, indicated by a square in the figure, is consistent with no signs of deep mixing, despite it clearly being the most evolved star in our study. The lack of an anticorrelation and the lack of variations seen in star 117 are consistent with a primordial variation for the differences in elemental abundances, presumably due to pollution during the earliest stages of the cluster formation and evolution by AGB nucleosynthesis and mass loss.

5.2. *The Other Light Elements:* Si, Ca, *and* Ti *Abundances*

Table 5 shows that the other light elements, silicon, calcium, and titanium, do not show any detectable variation in their abundances. These elements are of considerable interest

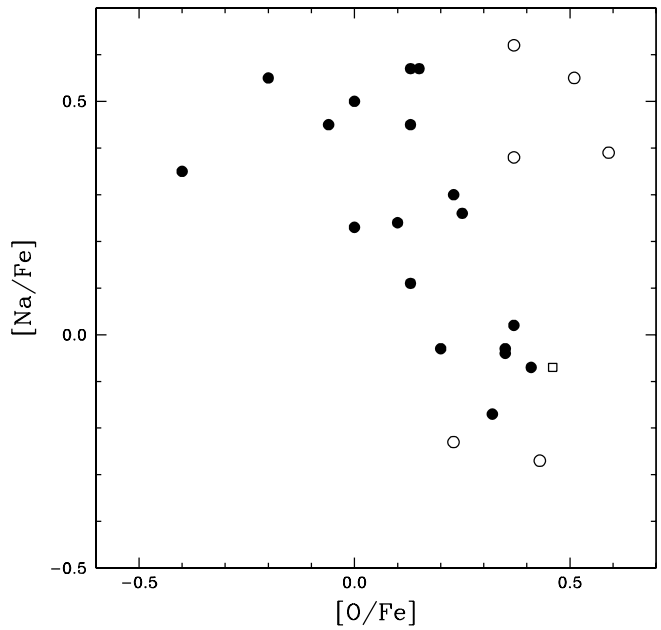

FIG. 6.—Comparison of [Na/Fe] vs. [O/Fe] for M15 (*filled circles*) vs. those of M68 (*open circles*). The post-AGB star M68-117 is marked with a square.

nonetheless because they provide us with an opportunity to compare the nucleosynthesis histories of clusters and, in principle, a means to compare the rate of star formation and, possibly, relative ages.

If star formation began everywhere in the Galaxy at about the same time, then the abundances of elements that emerge from Type II supernovae, including these light elements and *r*-process elements such as europium, will be enhanced relative to the abundances of elements that emerge from nucleosynthesis sites that appear more gradually, including *s*-process elements from AGB stars and iron-peak elements from Type Ia supernovae. The details are complex, but this picture is consistent with the basic behavior of these α-element abundances (see the discussions of Wyse & Gilmore 1988, Wheeler et al. 1989, and Carney 1996). If we compute unweighted averages for silicon, calcium, and titanium, we find for M68 that $[\alpha/\mathrm{Fe}] = +0.34 \pm 0.22$, which is roughly consistent with that found in M15 and other globular clusters. In Table 10, we summarize the [Si/Fe], [Ca/Fe], [Ti/Fe], and the mean $[\alpha/\mathrm{Fe}]$ ratios of M68, other globular clusters (Gratton 1987; Gratton & Ortolani 1989; Kraft et al. 1992, 1995, 1997, 1998; McWilliam et al. 1992; Sneden et al. 1994, 1997, 2000b; Brown et al. 1997, 1999; Ivans et al. 1999; Shetrone & Keane 2000), and field stars with $-2.50 \leq [\mathrm{Fe/H}] \leq -1.90$ studied by Fulbright (2000). (The errors are those of the mean.) In the table, old inner halo clusters denote metal-poor inner halo clusters NGC 6287 ([Fe/H] = −2.01), NGC 6293 (−1.99), and NGC 6541 (−1.76), and their Galactocentric distances are 1.6, 1.4, and 2.2 kpc, respectively (Lee & Carney 2002). The mean values of $[\alpha/\mathrm{Fe}]$ do not appear to vary much and are probably consistent within the internal errors (the simple averages) and any lingering systematic errors.

A closer examination of the abundances of these elements does reveal some interesting differences, however. The silicon abundance of M68 appears to be similar to that found in M15, and in both it is enhanced relative to that of other clusters and field stars.

The calcium abundance of M68 is likewise similar to that found in M15, and in both it is similar to other halo stars and clusters. There may, however, be a modest difference (≈0.15 dex) between M68, M15, and other old halo clusters and "younger halo" and thick-disk clusters. Note that this contradicts the assignment of M68 to the "younger halo" category.

On the other hand, the titanium abundance of M68 appears to be much lower than all other clusters. Is this effect real? The titanium abundance of the metal-poor RGB stars using the neutral titanium lines may suffer from NLTE effects, such as an overionization, and the resultant Ti abundance may be spurious. However, our Ti abundance analyses using the Ti II lines also yields a lower titanium abundance for our program stars, indicating that they are truly titanium deficient. In Figure 7, we show comparisons of observed spectrum of star 93 with those of synthetic spectra near Si I λ5665.56 and Ti I $\lambda\lambda$6258.11, 6258.71, and 6261.11. In the figure, the observed spectrum is represented by histograms, synthetic spectra with [Si/Fe] = +0.68, [Ti/Fe] = +0.06 by solid lines (see also Table 5), and synthetic spectra with [Si/Fe] = +0.30, [Ti/Fe] = +0.30, which elemental abundances have long been thought to be *normal* (if there exists normal elemental abundances among globular clusters) for globular clusters, by dotted lines. The observed spectrum clearly shows that the Si I absorption line is too strong to be [Si/Fe] = +0.30, while the Ti I absorption lines are too weak to be [Ti/Fe] = +0.30. So the deficiency appears to be real.

While we have included this element because its abundances often track those of the lighter elements, including oxygen,

TABLE 10
COMPARISONS OF α-ELEMENT ABUNDANCES

Object	[Si/Fe]	[Ca/Fe]	[Ti/Fe]	$[\alpha/\mathrm{Fe}]$	n[a]
M68	0.73 ± 0.02	0.31 ± 0.02	−0.03 ± 0.04	0.34 ± 0.22	5, 7, 7
M15[b]	0.62 ± 0.06	0.24 ± 0.01	0.27 ± 0.08	0.38 ± 0.12	11, 18, 4
Old halo	0.38 ± 0.05	0.30 ± 0.03	0.33 ± 0.03	0.34 ± 0.02	15
Old inner halo[c]	0.56 ± 0.05	0.26 ± 0.07	0.15 ± 0.06	0.32 ± 0.03	3
Younger halo	0.29 ± 0.09	0.14 ± 0.06	0.17 ± 0.07	0.20 ± 0.05	7
Younger halo[d]	0.38 ± 0.09	0.21 ± 0.04	0.25 ± 0.06	0.28 ± 0.02	5
Disk	0.39 ± 0.08	0.16 ± 0.07	0.31 ± 0.08	0.29 ± 0.04	4
Field[e]	0.52 ± 0.04	0.35 ± 0.03	0.30 ± 0.04	0.39 ± 0.02	9, 20, 20

[a] Number of stars (M68; M15; field) or clusters.
[b] We used [Si/Fe] and [Ca/Fe] from Sneden et al. (1997). For [Ti/Fe], we also employed data from Sneden et al. (2000a). We did not include any stars with uncertain measures (marked with a colon in their results).
[c] NGC 6287, 6293, and 6541 (Lee & Carney 2002).
[d] Without Pal 12 and Ruprecht 106.
[e] Mean abundances for field stars with $-2.50 \leq [\mathrm{Fe/H}] \leq -1.90$.

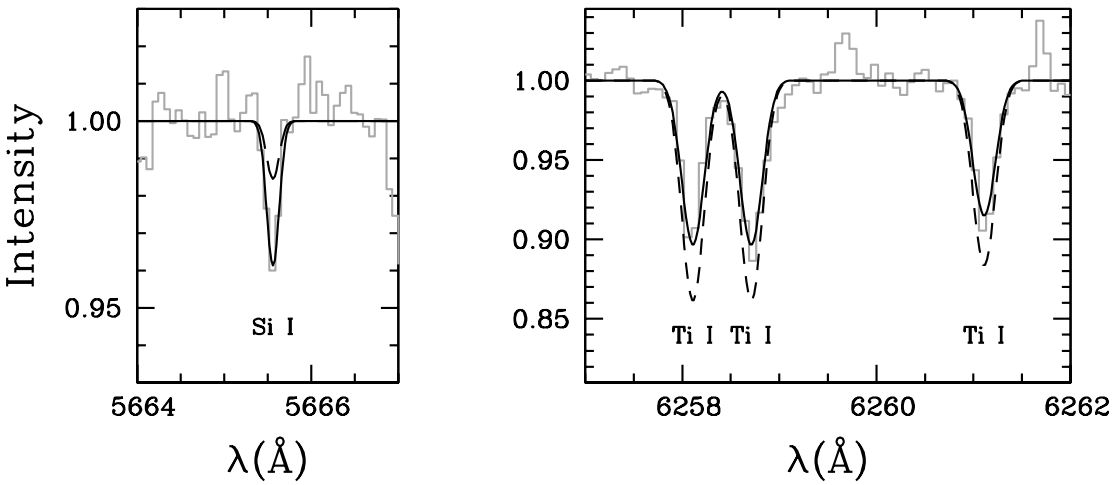

FIG. 7.—Comparisons of observed spectrum of the star M68-93 with those of synthetic spectra near Si I λ5665.56 and Ti I $\lambda\lambda$6258.11, 6258.71, and 6261.11. The observed spectrum is presented by histograms, synthetic spectra with [Si/Fe] = +0.68, [Ti/Fe] = +0.06 by solid lines (see also Table 5), and synthetic spectra with [Si/Fe] = +0.30, [Ti/Fe] = +0.30 by dotted lines.

magnesium, silicon, and calcium, titanium may also be considered to be an iron-peak element. Explosive nucleosynthesis calculations of the massive stars (Woosley & Weaver 1995) predict that one of the major sources of the SNe II titanium yield is ^{48}Cr via the consecutive electron capture processes. Furthermore, their models predicted that SNe II with masses in the range 25–40 $M_\odot$ are likely to overproduce Si compared with Ti. We turn, therefore, to a more detailed comparison between M68 and M15, concentrating on the light element silicon, thought to be mostly produced in Type II supernovae, and nickel, mostly associated with Type Ia supernovae. Sneden et al. (1997) also found a high silicon abundance in M15. Restricting the sample to only those stars with well-determined abundances, they found $\langle$[Si/Fe]$\rangle = +0.62 \pm 0.06$. Again using only the stars with well-determined titanium abundances and comparing [Ti I/Fe I] and [Ti II/Fe II], the four stars studied by Sneden et al. (1997, 2000a) resulted in $\langle$[Ti/Fe]$\rangle = +0.27 \pm 0.08$ (the errors are all given here as errors of the mean). Thus, for M15, [Si/Ti] is +0.35, whereas for M68 it is much higher, +0.76. For the iron-peak element nickel, our seven stars reveal $\langle$[Ni/Fe]$\rangle = -0.11 \pm 0.03$ ($\sigma = 0.08$) dex. We are uncertain how to compare our results with those from Sneden et al. (1997, 2000a), however. Sneden et al. (1997) found $\langle$[Ni/Fe]$\rangle = +0.14 \pm 0.03$, on the basis of 12 stars, which is very different from what we found for M68. But Sneden et al. (2000a) found $\langle$[Ni/Fe]$\rangle = -0.21 \pm 0.02$ ($\sigma = 0.04$) dex, on the basis of three of the same stars studied earlier. Sneden et al. (2000a) commented on the difficulties in establishing truly reliable stellar parameters and abundances, and, alas, this difference is yet another aspect of that problem.

We conclude our discussion of these elements by mentioning the possibility that the stars we have studied in M68 sampled a relatively high end of the IMF and the resulting supernovae.

5.3. *The Heavy Neutron Capture Elements* Ba, La, *and* Eu

The elements heavier than the iron-peak elements cannot be efficiently produced by charged-particle interactions because of large Coulomb repulsion between the nuclei, and they are thought to be produced through both slow (*s*-) and rapid (*r*-) neutron capture processes. The *s*-process occurs mainly in low- (1–3 $M_\odot$) or intermediate-mass (4–7 $M_\odot$) AGB stars, while the *r*-process is thought to occur in Type II supernovae explosions. Therefore, comparisons between the *r*-process (europium) and *s*-process elements (barium and lanthanum) provide a clue to the history of Galactic nucleosynthesis, since *r*- and *s*-processes are thought to occur in stars with very different masses and therefore at different points in the evolutionary timescale.

Burris et al. (2000) studied abundances of neutron capture elements in a large sample of metal-poor giants, finding that a large star-to-star variations in the neutron capture elemental abundances (see also Gilroy et al. 1988 and McWilliam et al. 1995). They suggested that this scatter in neutron capture elemental abundances results from inhomogeneity in the protostellar material, which was polluted by SNe II nucleosynthesis ejecta at an early stage in the Galaxy's history. Whether this is the correct interpretation or whether the analyses themselves are partly responsible for the scatter remains to be seen (see Cayrel et al. 2004). In Figure 8, we show Ba, La, and Eu abundances for globular clusters (Brown et al. 1997, 1999; Gratton et al. 1986; Gratton 1987; Gratton & Ortolani 1989; Ivans et al. 1999, 2001; Kraft et al. 1998; Lee & Carney 2002; McWilliam et al. 1992; Shetrone & Keane 2000; Sneden et al. 1997, 2000a, 2000b, 2004) and field stars (Burris et al. 2000) as a function of metallicity. Table 11 summarizes mean Ba, La, and Eu abundances for M68 and M15 (Sneden et al. 1997, 2000a), other globular clusters, and field stars with $-2.50 \leq$ [Fe/H] ≤ -1.90 (Burris et al. 2000).

The comparison with M15 and other clusters and stars is not quite as simple, however, as it appears. Sneden et al. (1997) discovered that whereas the abundances of the lighter elements silicon, calcium, and titanium did not vary from star to star, those of the neutron capture elements did, and by factors of 4 to 5. Like the variation in [Si/Ti] seen between M68 and other clusters, the variations in [Ba/Fe] and [Eu/Fe] seen by Sneden et al. (1997, 2000a) warn us not to assume that all supernovae produce the same heavy-element abundance yields. In the case of M15, the lack of variations in the abundances of the light elements would predict in such a simple model that barium and other *s*-process elements and the *r*-process element europium should likewise be constant, contrary to what was seen.

How does M68 fit into this picture? In Figure 9 we reproduce the [Ba/Fe] versus the [Eu/Fe] abundances found by Sneden et al. (1997). The dotted line shows the solar abundances, and the dashed line, displaced from the solar relation by 0.41 dex,

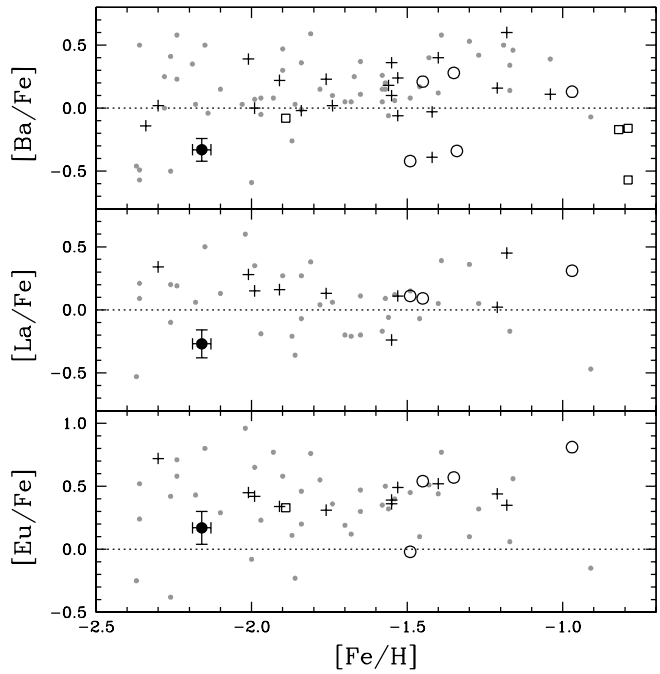

FIG. 8.—Abundances of the neutron capture elements. Plus signs are old halo clusters, open circles younger halo clusters; squares are thick-disk clusters, and gray dots field stars (Burris et al. 2000). M68 is represented by filled circles.

shows the mean behavior of the stars in M15 (*plotted as dots*). As Sneden et al. (1997) noted, the behavior of the stars in M15 is consistent with an enhanced *r*-process contribution to the abundances of *both* barium and europium in M15. That process produced different absolute amounts of the neutron capture elements in stars in M15, but the process itself yielded the same relative abundances of the two elements. Our results for the stars in M68 are consistent with this general picture, in that the barium and europium abundance ratio is constant and essentially the same in M68 and in M15. Sneden et al. (1997) found that the "low-barium" and "high-barium" groups of stars in M15 had similar [Ba/Eu] ratios, -0.41 ± 0.03 ($\sigma = 0.13$) dex, for all eighteen stars. Our seven stars, including the post-AGB star 117, yield $\langle$[Ba/Eu]$\rangle = -0.43 \pm 0.05$ ($\sigma = 0.13$) dex. What *is* different between the two clusters, however, is that both barium and europium are lower in abundance in M68 than in the stars in M15, even the "low-barium" stars. Thus, M68 was slightly less enriched in *r*-process nucleosynthesis relative to iron. We could interpret our results in an alternative fashion, arguing that iron is enhanced relative to the *r*-process elements, in this case including barium and europium.

For [La/Eu] we must turn to the smaller sample of Sneden et al. (2000a), who studied three stars in M15 with very different [Ba/Fe] ratios, −0.24, +0.05, and +0.05. The [La/Fe]-values also vary greatly for these three stars, −0.02, +0.38, and +0.61, yet the variation seen in [La/Eu] is much smaller and is consistent with the measurement uncertainties, −0.33, −0.45, and −0.26, for a mean value of -0.35 ± 0.06 ($\sigma = 0.10$) dex. We were able to estimate [La/Eu]-values for three of our program stars, and we find $\langle$[La/Eu]$\rangle = -0.38 \pm 0.10$ ($\sigma = 0.17$) dex. Thus, for both lanthanum and barium, it appears the *r*-process dominates nucleosynthesis enrichment in both M68 and in M15 and yields constant relative abundances of the elements. But, as in the case of barium and europium, there is an underabundance of lanthanum relative to iron in M68 compared with M15.

5.4. *Summary of Differences Between M68 and M15 and Other Clusters*

In Figure 10, we summarize graphically the many similarities between the abundances of various elements relative to iron in M68 compared with M15. Perhaps the two most striking differences are in the much lower titanium abundances in M68, which, as we have seen, might be explained by a greater contribution from more massive stars and their supernovae events in M68 relative to M15. On the other hand, while it appears that the *r*-process has dominated the production of the "traditional" *s*-process elements lanthanum and barium and that the [La/Eu] and [Ba/Eu] ratios are the same for all the stars in both clusters, the overall *r*-process enrichment varies within M15 (Sneden et al. 1997) and between M68 and M15. The clusters have clearly experienced somewhat different chemical enrichment histories, and it will be interesting to see whether models of supernovae enrichment ultimately prove successful in explaining these differences and what this means for the histories and, perhaps, ages of these clusters.

TABLE 11
COMPARISONS OF NEUTRON CAPTURE ELEMENT ABUNDANCES

Object	[Ba/Fe]	*n*	[La/Fe]	*n*	[Eu/Fe]	*n*[a]
M68	−0.31 ± 0.08		−0.27 ± 0.11		+0.20 ± 0.13	7, 3, 6
M15-all[b]	+0.10 ± 0.21		...		+0.49 ± 0.20	18, 0, 18
M15-high Ba[c]	+0.23 ± 0.09		...		+0.66 ± 0.08	10, 0, 10
M15-low Ba[d]	−0.11 ± 0.06		...		+0.29 ± 0.09	8, 0, 8
Old halo	+0.11 ± 0.23	16	+0.22 ± 0.18	5	+0.45 ± 0.13	8
Old inner halo[e]	+0.21 ± 0.20	3	+0.18 ± 0.08	3	+0.39 ± 0.07	3
Younger halo	−0.03 ± 0.33	5	+0.17 ± 0.12	3	+0.48 ± 0.35	4
Younger halo[f]	+0.05 ± 0.34	3	+0.09	1	+0.56 ± 0.02	2
Disk	−0.25 ± 0.22	4	...	...	+0.33	1
Field[g]	+0.18 ± 0.11	27	+0.11 ± 0.08	14	+0.39 ± 0.09	17

[a] Number of stars (M68; M15; field) or clusters.
[b] Sneden et al. (1997).
[c] High-Ba group (Sneden et al. 1997). See Fig. 9.
[d] Low-Ba group (Sneden et al. 1997). See Fig. 9.
[e] NGC 6287, 6293, and 6541 (Lee & Carney 2002).
[f] Without Pal 12 and Ruprecht 106.
[g] Mean abundances for field stars with $-2.50 \leq$ [Fe/H] ≤ -1.90 (Burris et al. 2000).

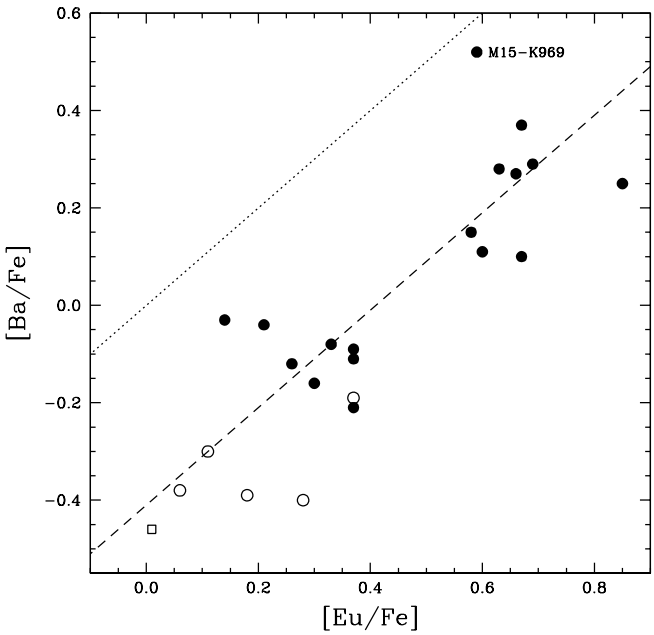

FIG. 9.—Abundances of barium and europium relative to iron in M15 (*filled circles*) and M68 (*open circles*). The post-AGB star M68-117 is marked by an square. The dotted line represents the solar abundance pattern. The dashed line is the approximate mean for the stars in M15. Despite varying levels of neutron capture abundances in the cluster, the [Ba/Eu] ratio appears to be constant. That is true as well for M68.

Finally, in Figure 11 we show the results for individual stars in the abundance ratio of barium and europium plotted against [Ca/H], rather than [Fe/H]. As Sneden et al. (1997) commented, calcium is thought to be produced in Type II supernovae, compared with iron, whose abundance is more strongly affected by contributions from Type Ia supernovae. Also following Sneden et al. (1997), we show the levels expected from "pure" *r*-process nucleosynthesis, "pure" *s*-process nucleosynthesis, and the intermediate case found to exist in the solar system. At lower [Ca/H] levels, [Ba/Eu] ratios more consistent with *r*-process domination are apparent, which is not terribly surprising. But M68 appears to be one of the most extreme cases.

6. CONCLUSIONS

A chemical abundance study of seven giant stars in M68 has been presented. We estimate the stars' temperatures using the

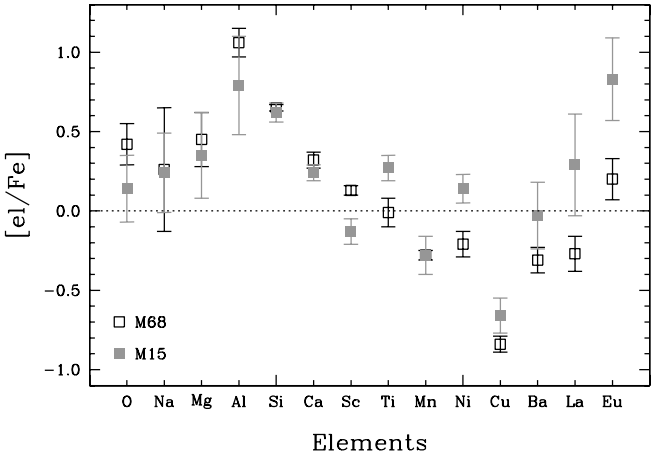

FIG. 10.—Comparison of elemental abundances between M68 and M15.

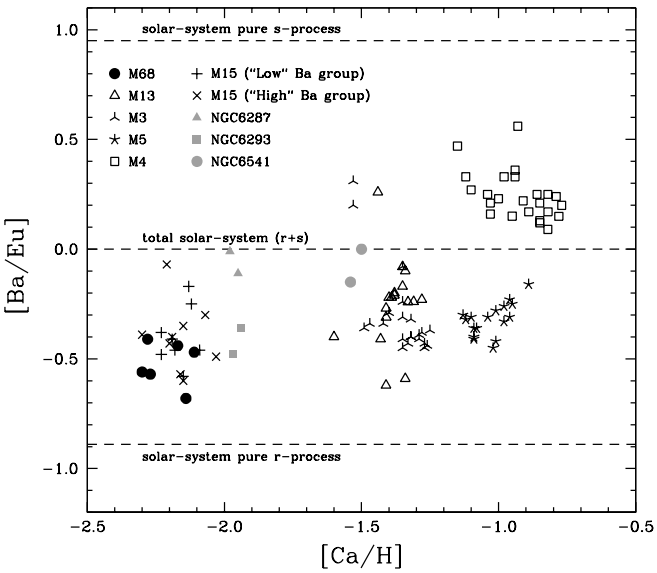

FIG. 11.—Comparisons of [Ba/Eu] ratios as a function of [Ca/H] of our program stars in M68 and individual stars in other globular clusters.

abundances derived from Fe I lines with differing excitation potentials, but the gravity has been derived using available photometry rather than a comparison between abundances from pressure-insensitive Fe I lines and pressure-sensitive Fe II lines. The "spectroscopic" gravities do not agree with the photometric gravities, suggesting that NLTE effects are present. Using only the Fe II lines, which should be less sensitive to NLTE and photometric gravities, we find $[\mathrm{Fe/H}] = -2.16 \pm 0.02$ ($\sigma = 0.04$). We have compared our results with those of Gratton & Ortolani (1989), who found a higher value. We attribute the difference to the lower resolution spectra available to them at the time. Our results do agree well with those obtained by Minniti et al. (1993), but we regard the agreement as accidental, since we could not reproduce their results using their data.

We determine element-to-iron ratios using neutral versus neutral and ionized versus ionized lines to again minimize NLTE effects. We find a large range in sodium abundances but no significant range in oxygen abundances. Furthermore, the post-AGB star M68-117 does not appear to show any enhancement of sodium. These results are not consistent with deep mixing being the cause of the variations among the light elements oxygen, sodium, magnesium, and aluminum.

There are two notable differences between M68 and the comparably metal-poor cluster M15. While both show enhanced [Si/Fe] ratios relative to other clusters and comparably metal-poor field stars, M68 is quite deficient in titanium compared with M15 or any other cluster. It is possible that this arose because the nucleosynthesis enrichment of the stars in M68 was provided by supernovae resulting from the deaths of somewhat more massive progenitors. This would be difficult to reconcile with the nominal younger age for M68 compared with M15, on the basis of the morphologies of their HB stars' distribution in temperature/color. Perhaps age is not the only "second parameter."

The second interesting difference is that the [La/Eu] and [Ba/Eu] ratios are similar for the stars in M68 and in M15 (and in both its high-barium and low-barium groups of stars; Sneden et al. 1997). This suggests that in both clusters the *r*-process makes a major contribution to the abundance levels of the "traditional" *s*-process elements lanthanum and barium.

However, whatever the process is, it does not contribute quite as much to the neutron capture element abundances in M68 as in M15.

This research was supported by NASA grant GO-07318.04-96A from the Space Telescope Science Institute, which is operated by AURA, Inc., under NASA contract NAS5-26555. We also thank the NSF for financial support via grants AST 96-19381, AST 98-88156, and AST 03-0541 to the University of North Carolina. Support for this work was also provided by the Korea Science and Engineering Foundation to the Astrophysical Research Center for the Structure and Evolution of the Cosmos.

REFERENCES

Alcaino, G. 1977, A&AS, 29, 9
Allende Prieto, C., García López, R., Lambert, D. L., & Gustafsson, B. 1999, ApJ, 527, 879
Alonso, A., Arribas, S., & Martinez-Roger, C. 1998, A&AS, 131, 209
———. 1999, A&AS, 140, 261
Bard, A., & Kock, M. 1994, A&A, 282, 1014
Bard, A., Kock, A., & Kock, M. 1991, A&A, 248, 315
Bellazzini, M., Ferraro, F. R., & Ibata, R. 2002, AJ, 124, 915
Bellazzini, M., Ibata, R., Ferraro, F. R., & Testa, V. 2003, A&A, 405, 577
Biémont, E., Baudous, M., Kurucz, R. L., Ansbacher, W., & Pinnington, E. H. 1991, A&A, 249, 539
Biémont, E., Karner, C., Meyer, G., Traeger, F., & Zu Putlitz, G. 1982, A&A, 107, 166
Blackwell, D. E., Booth, A. J., Haddock, D. J., Petford, A. D., & Leggett, S. K. 1986a, MNRAS, 220, 549
Blackwell, D. E., Booth, A. J., Menon, S. L. R., & Petford, A. D. 1986b, MNRAS, 220, 289
Blackwell, D. E., Menon, S. L. R., & Petford, A. D. 1983, MNRAS, 204, 883
Blackwell, D. E., Menon, S. L. R., Petford, A. D., & Shallis, M. J. 1982a, MNRAS, 201, 611
Blackwell, D. E., Petford, A. D., Shallis, M. J., & Simmons, G. J. 1982b, MNRAS, 199, 43
Blackwell, D. E., Petford, A. D., & Simmons, G. J. 1982c, MNRAS, 201, 595
Blackwell, D. E., Smith, G., & Lynas-Gray, A. E. 1995, A&A, 303, 575
Brown, J. A., Wallerstein, G., & Gonzalez, G. 1999, AJ, 118, 1245
Brown, J. A., Wallerstein, G., & Zucker, D. 1997, AJ, 114, 180
Burris, D. L., Pilachowski, C. A., Armandroff, T. E., Sneden, C., Cowan, J. J., & Roe, H. 2000, ApJ, 544, 302
Carney, B. W. 1996, PASP, 108, 900
Carretta, E., Gratton, R. G., Bragaglia, A., Bonifacio, P., & Pasquini, L. 2004, A&A, 416, 925
Cayrel, R., et al. 2004, A&A, 416, 1117
Cohen, J. G. 2004, AJ, 127, 1545
Cutri, R. M., et al. 2000, 2MASS Second Incremental Data Release (Pasadena: Caltech)
Da Costa, G. S., & Armandroff, T. E. 1995, AJ, 109, 2533
Dinescu, D. I., Girard, T. M., & van Altena, W. F. 1999, AJ, 117, 1792
Dinescu, D. I., Majewski, S. R., Girard, T. M., & Cudworth, K. M. 2000, AJ, 120, 189
Freeman, K. 1993, in ASP Conf. Ser. 265, ω Centauri: A Unique Window into Astrophysics, ed. F. van Leeuwen, J. D. Hughes, & G. Piotto (San Francisco: ASP), 365
Freeman, K., & Bland-Hawthorn, J. 2002, ARA&A, 40, 487
Frogel, J. A., Persson, S. E., & Cohen, J. G. 1983, ApJS, 53, 713
Fuhr, J. R., Martin, G. A., & Wiese, W. L. 1988a, Atomic Transition Probabilities. Scandium through Manganese, Vol. 17, No. 3 (New York: AIP/ACS)
———. 1988b, Atomic Transition Probabilities. Iron through Nickel, Vol. 17, No. 4 (New York: AIP/ACS)
Fulbright, J. P. 2000, AJ, 120, 1841
Garz, T. 1973, A&A, 26, 471
Gilroy, K. K., Sneden, C., Pilachowski, C. A., & Cowan, J. J. 1988, ApJ, 327, 298
Gratton, R. G. 1987, A&A, 179, 181
Gratton, R. G., et al. 2001, A&A, 369, 87
Gratton, R. G., & Ortolani, S. 1989, A&A, 211, 41
Gratton, R. G., Quarta, M. L., & Ortolani, S. 1986, A&A, 169, 208
Grevesse, N., Blackwell, D. E., & Petford, A. D. 1989, A&A, 208, 157
Harris, W. E. 1975, ApJS, 29, 397
———. 1996, AJ, 112, 1487
Ivans, I. I., Kraft, R. P., Sneden, C., Smith, G. H., Rich, R. M., & Shetrone, M. 2001, AJ, 122, 1438
Ivans, I. I., Sneden, C., Kraft, R. P., Suntzeff, N. B., Smith, V. V., Langer, G. E., & Fulbright, J. P. 1999, AJ, 118, 1273
Kraft, R. P. 1994, PASP, 106, 553
Kraft, R. P., & Ivans, I. I. 2003, PASP, 115, 143
Kraft, R. P., Sneden, C., Langer, G. E., & Prosser, C. F. 1992, AJ, 104, 645
Kraft, R. P., Sneden, C., Langer, G. E., Shetrone, M. D., & Bolte, M. 1995, AJ, 109, 2586
Kraft, R. P., Sneden, C., Smith, G. H., Shetrone, M. D., & Fulbright, J. 1998, AJ, 115, 1500
Kraft, R. P., Sneden, C., Smith, G. H., Shetrone, M. D., Langer, G. E., & Pilachowski, C. A. 1997, AJ, 113, 279
Kurucz, R. 1993, CD-ROM 1, Atomic Data for Opacity Calculations (Cambridge: Smithsonian Astrophys. Obs.)
Lambert, D. L. 1978, MNRAS, 182, 249
Lee, J.-W., & Carney, B. W. 2002, AJ, 124, 1511
Lee, Y.-W., Demarque, P., & Zinn, R. 1990, ApJ, 350, 155
———. 1994, ApJ, 423, 248
Livingston, C. W. 1999, in Allen's Astrophysical Quantities (4th ed.; New York: Springer), 339
Lynden-Bell, D., & Lynden-Bell, R. M. 1995, MNRAS, 275, 429
Majewski, S. R., et al. 2004, AJ, 128, 245
McWilliam, A. 1997, ARA&A, 35, 503
———. 1998, AJ, 115, 1640
McWilliam, A., Geisler, D., & Rich, R. M. 1992, PASP, 104, 1193
McWilliam, A., Preston, G. W., Sneden, C., & Searle, L. 1995, AJ, 109, 2757
Minniti, D., Geisler, D., Peterson, R. C., & Claria, J. J. 1993, ApJ, 413, 548
Minniti, D., Peterson, R. C., Geisler, D., & Claria, J. J. 1996, ApJ, 470, 953
Nissen, P. E., Hoeg, E., & Schuster, W. J. 1997, *Hipparcos*-Venice '97, ed. B. Battrick, et al. (ESA SP-402) (Noordwijk: ESA), 225
O'Brian, T. R., Wickliffe, M. E., Lawler, J. E., Whaling, W., & Brault, J. W. 1991, J. Opt. Soc. Am. B, 8, 1185
Prochaska, J. X., & McWilliam, A. 2000, ApJ, 537, L57
Rey, S.-C., Yoon, S.-J., Lee, Y.-W., Cahboyer, B., & Sarajedini, A. 2001, AJ, 122, 3219
Rosenberg, A., Saviane, I., Piotto, G., & Aparicio, A. 1999, AJ, 118, 2306
Rutledge, G. A., Hesser, J. E., & Stetson, P. B. 1997, PASP, 109, 907
Searle, L., & Zinn, R. 1978, ApJ, 225, 357
Shetrone, M. D., & Keane, M. J. 2000, AJ, 119, 840
Simmerer, J., Sneden, C., Ivans, I. I., Shetrone, M. D., & Smith, V. V. 2003, AJ, 125, 2018
Smith, G. 1981, A&A, 103, 351
Smith, V. V., Suntzeff, N. B., Cunha, K., Gallino, R., Busso, M., Lambert, D. L., & Straniero, O. 2000, AJ, 119, 1239
Sneden, C. 1973, Ph.D. thesis, Univ. Texas, Austin
Sneden, C., Johnson, J., Kraft, R. P., Smith, G. H., Cowan, J. J., & Bolte, M. S. 2000a, ApJ, 536, L85
Sneden, C., Kraft, R. P., Guhathakurta, P., Peterson, R. C., & Fulbright, J. P. 2004, AJ, 127, 2162
Sneden, C., Kraft, R. P., Langer, G. E., Prosser, C. F., & Shetrone, M. D. 1994, AJ, 107, 1773
Sneden, C., Kraft, R. P., Prosser, C. F., & Langer, G. E. 1991, AJ, 102, 2001
Sneden, C., Kraft, R. P., Shetrone, M. D., Smith, G. H., Langer, G. E., & Prosser, C. F. 1997, AJ, 114, 1964
Sneden, C., Pilachowski, C. A., & Kraft, R. P. 2000b, AJ, 120, 1351
Thévenin, F., & Idiart, T. P. 1999, ApJ, 521, 753
VandenBerg, D. A. 2000, ApJS, 129, 315
Walker, A. R. 1994, AJ, 108, 555
Wheeler, J. C., Sneden, C., & Truran, J. W. 1989, ARA&A, 27, 279
Woosley, S. E., & Weaver, T. A. 1995, ApJS, 101, 181
Wyse, R. F. G., & Gilmore, G. 1988, AJ, 95, 1404
Yoon, S.-J., & Lee, Y.-W. 2002, Science, 297, 578
Zinn, R. 1985, ApJ, 293, 424
———. 1993, in ASP Conf. Ser. 48, The Globular Cluster–Galaxy Connection, ed. G. H. Smith & J. P. Brodie (San Francisco: ASP), 38
Zinn, R., Newell, E. B., & Gibson, J. B. 1972, A&A, 18, 390
Zinn, R., & West, M. J. 1984, ApJS, 55, 45